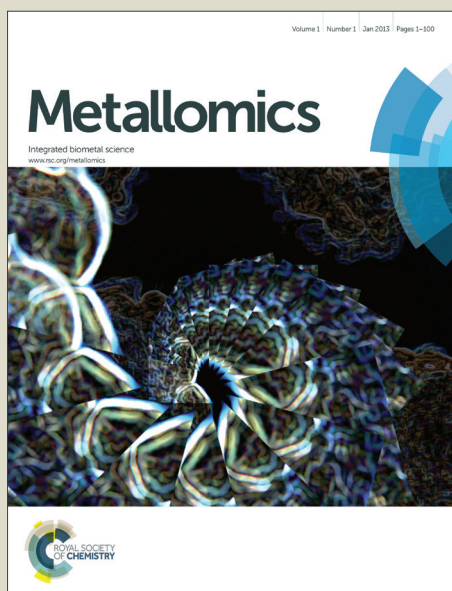


Metallomics

Accepted Manuscript



This is an *Accepted Manuscript*, which has been through the Royal Society of Chemistry peer review process and has been accepted for publication.

Accepted Manuscripts are published online shortly after acceptance, before technical editing, formatting and proof reading. Using this free service, authors can make their results available to the community, in citable form, before we publish the edited article. We will replace this *Accepted Manuscript* with the edited and formatted *Advance Article* as soon as it is available.

You can find more information about *Accepted Manuscripts* in the [Information for Authors](#).

Please note that technical editing may introduce minor changes to the text and/or graphics, which may alter content. The journal's standard [Terms & Conditions](#) and the [Ethical guidelines](#) still apply. In no event shall the Royal Society of Chemistry be held responsible for any errors or omissions in this *Accepted Manuscript* or any consequences arising from the use of any information it contains.

Cite this: DOI: 10.1039/c0xx00000x

www.rsc.org/xxxxxx

ARTICLE TYPE

Challenging Conventional Wisdom: Single Domain Metallothioneins

Duncan E. K. Sutherland and Martin J. Stillman*

Received (in XXX, XXX) Xth XXXXXXXXXX 20XX, Accepted Xth XXXXXXXXXX 20XX

DOI: 10.1039/b000000x

5

Metallothioneins (MT) are a family of small cysteine rich proteins that have been implicated in a range of roles including toxic metal detoxification, protection against oxidative stress, and as metallochaperones are undoubtedly involved in the homeostasis of both essential zinc and copper. While complete details of all possible cellular functions are still unknown, it is clear that they must be directly related to both the accessibility and the metal-binding properties of the many cysteine residues in the protein. The most well studied MTs are of mammalian origin and consist of two domains: a β -domain with 9 cysteine residues that sequesters 3 Cd^{2+} , 3 Zn^{2+} or 6 Cu^+ ions, and an α -domain with 11 cysteine residues that sequesters 4 Cd^{2+} , 4 Zn^{2+} or 6 Cu^+ ions. The key to understanding the cellular importance of MT in these different roles is in a precise description of the metallation status before and during reactions. An assessment of all possible and all biologically accessible metallation states is necessary before the functional mechanistic details can be fully determined. Conventionally, it has been considered that metal ions bind in a domain-specific and, therefore, cooperative manner, where the apparently isolated domains fill with their full complement of metal ions immediately with no discernible or measurable intermediates. A number of detailed mechanistic studies of the metallation reactions of mammalian MTs have provided significant insight into the metallation reactions. Recent results from electrospray ionization mass spectrometric studies of the stepwise metallation of the two fragments and the whole protein with Zn^{2+} , Cd^{2+} , As^{3+} and Bi^{3+} indicate a noncooperative mechanism of a declining series of K_F 's. Of particular note are new details about the early stages of the stepwise metallation reactions, specifically the stability of partially metallated species for As^{3+} , Cd^{2+} , and Zn^{2+} that do not correspond to the two-domain model. In addition, at the other end of the coordination spectrum are the supermetallated species of MT, where supermetallation defines metallation in excess of traditional levels. It has been reported that with metal ion excess the formation of a single 'super domain' is possible and again this deviates from the two-domain model of MT. In both cases, these results suggest that the structural view of mammalian MT that is of two essentially isolated domains may be the exceptional case and that under the normal conditions of cellular metal-ion concentrations the two domain structure might coexist in equilibrium with various single domain, multi-metal site structures. This review specifically focuses on providing context for these recent studies and the new ideas concerning metallation prior to the establishment of domain-based clusters that these studies suggest.

35

1. Metallothionein

Metallothioneins (MTs) are a group of metalloproteins typically characterized by their small size, high cysteine content (~30%), absence of disulfide bonds, and lack of aromatic amino acids¹⁻³. However, while this description is commonly applied to MTs, new species have been documented to contain cysteine rich proteins that contain aromatic amino acids⁴⁻⁶. The metal-thiolate

bond and eventual cluster formation dominates the metallation chemistry of MT and both the secondary and tertiary structure is formed as a result of metal-ion coordination⁷⁻⁹. Metallation of metallothioneins is an example of metal-induced folding. Cd-MT was initially isolated by Margoshes and Vallee in 1957 from samples of horse kidney cortex that through progressive purification showed an increase in relative cadmium content¹⁰. The protein was named metallothionein for its unusually high metal (metallo) and sulphur (thiol) content. Since its discovery,

members of the MT family have been isolated from a wide array of sources including all animal phyla, fungi, plants, as well as cyanobacteria, proteobacteria and actinobacteria¹¹⁻¹⁴. As a result of MT's existence across all kingdoms in Nature, a large number of examples of MTs have been characterized including some that do contain aromatic amino acids, e.g. tyrosines and histidines, that were previously called class II MTs, and that also may contain variable cysteine content. Several of these species are included in the discussion below illustrating the complexity of the MT family. The ubiquitous nature of MT, coupled with its ability to coordinate a several metal ions of both the same identity and mixed identities has implicated this class of protein in many physiological processes¹⁵⁻¹⁷. The most commonly cited processes are metal ion homeostasis, toxic metal detoxification, and protection against oxidative stress.

The initial reports of a kidney protein containing 7 Cd metal ions from Margoshes, Kagi and Vallee provided the groundwork for an intense interest in characterization studies, which culminated in the ¹¹³Cd NMR reports showing clusters were involved for at least Cd-MT¹⁸⁻²⁰. Following this discovery, coincident reports of both the X-ray and ¹H NMR structure showed the overall peptide wrapping and cluster alignment²¹. Subsequently, a large number of metallation studies using a range of spectroscopic techniques built up a picture of the properties of the two-domain structure that included the possible domain-specificity for different metals being exhibited by the α - or β -metal binding domains within the whole protein^{1,22}. Therefore, the typical view of MT has become that of two isolated but linked domains that are capable of independently filling in an order that is dependent on the identity of the incoming metal ion. This paradigm has been the driving focus of the analysis of many metallation and structural studies, including our own using CD and emission spectral data²³⁻²⁸.

More recently, four specific examples of single domain MTs have been reported, the best characterized being that of copper MT from yeast where the X-ray structure showed a mixture of digonally- and trigonally-coordinated Cu²⁺²⁹. This is a protein metallated to its nominal saturation. The second example is that of the supermetallation of human rhMT-1 with Cd²⁺ that resulted in a single domain, this time the 8th Cd²⁺ caused the two domains to rearrange into a single, coalesced domain³⁰. The third example encompasses MT from a number of different sources, namely the binding of As³⁺ to, as a single case, apo-rhMT-1. The metallated structure is devoid of bridging cysteinyl thiolates and so can be understood in terms of a single domain holding 6 As³⁺ ions in a beaded structure of terminal cysteinyl thiols.³¹⁻³⁴ The fourth example, is the very recent description of Zn²⁺ binding to apo-rhMT-1 studied by ESI-mass spectrometry in which a single domain, beaded structure is proposed up to the Zn₅-MT-1 point, after which clustering starts for the 6th and 7th Zn²⁺ added.³⁵⁻³⁷

This review is concerned with the impact on our understanding of the overall process of the metallation of metallothioneins following the combined reports of the single domain Cu-MT from yeast and the Cd₈-hMT 1a, and then the As³⁺ and most recently the new Zn²⁺ metallation studies, one a kinetic and the other an equilibrium study³¹⁻³⁷. Both of these latter studies required a view of the process that does not follow the traditionally accepted mechanism. Our discussion has as its

starting point the process of taking a single metal-free peptide strand and successively adding metal-ions (for example, in this case As³⁺) until saturation is achieved.

Initially, 20 cysteine residues are available for metal-ion coordination in the apo-MT protein. Many of these cysteines are either immediately adjacent to each other, or separated by only a few amino acids. It is, therefore, not surprising that the first metals added are predicted to bind using terminal cysteinyl thiolate ligands. For As³⁺ only three cysteinyl thiols will bind. So it is through the analysis of As³⁺ metallation studies that it has been possible to interpret the ESI-mass spectrometric data completely. As³⁺ does not form clusters with the cysteinyl thiols of MT, as far as we can determine.³⁸ The end-point for As-MT is that of 6 As³⁺ coordinated using only terminal thiolates as shown in the computational model of Ngu, *et al.*³¹⁻³⁴ Thus the As-MT metallation mechanism may be seen as metallation of a single domain protein with six bead-like sites and as such is an ideal system for determining the characteristics that one would expect to observe in a nonbridging metallated species that is in a single domain protein.

The involvement of terminal cysteines initially to form MS₃ or MS₄ bead-like metal binding sites follows the expected thermodynamically most preferred structures, where the bonding involves 3 or 4 M-SR bonds. The significant contention in the literature is at which point the clusters are formed^{35, 37, 39-41}. The metallation mechanism may be described as cooperative if cluster formation is complete in one domain before the other domain is metallated. On the other hand the mechanism may be described as non-cooperative if the clustered domains form only when all terminally coordinated sites are filled. That would be a single domain with 5 sites when the divalent Zn²⁺ and Cd²⁺ bind to the 20 cysteinyl thiols of mammalian MT and would represent the first metal-saturated state. This would be a metallated state with no free cysteine residues but also no traditional (for MTs) α - or β -clusters. Finally, with the two additional equivalents of zinc ions, the clustered fully metallated state (containing both bridging and terminal thiolate ligands) would be formed (Figure 1).

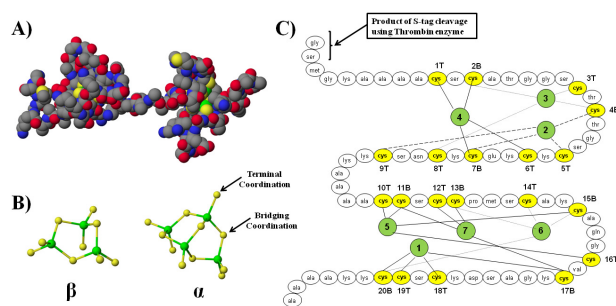


Figure 1. Three-dimensional structure and sequence-metal-binding alignment of Cd₇-MT-1. (A) A space-filling structure of Cd₇- β -rhMT-1. The N-terminal β -domain is located on the left-hand side, while the C-terminal α -domain is located on the right-hand side. (B) Cadmium-cysteinyl-thiolate clusters of Cd₇- β -rhMT-1 presented as ball and stick models: β -domain (left) and α -domain (right). (C) A metal connectivity diagram for MT-1 based on the sequence and the presence of 7, tetrahedrally coordinated metals. Each of the seven cadmium atoms is connected to exactly four cysteine amino acids. The connectivity

diagram has been renumbered from the original to emphasize the location and the coordination environment of each cysteine residue, where a T signifies terminal coordination to a single cadmium atom and a B signifies bridging coordination to two distinct cadmium atoms. Numbering of the Cd-thiolate centres is based on the NMR assignment by Messerle *et al.*⁶⁸ Reprinted with permission from Sutherland *et al.*³⁰ copyright (2012) American Chemical Society.

Based on the detailed analysis of stepwise Zn²⁺ binding we have proposed that the bead formation exemplified by that As₆-MT structure is the norm prior to cluster formation. Indeed, the bead structure invokes reasonable thermodynamic arguments where for Zn²⁺ four terminal thiolates form a strong tetrahedral complex with the divalent metals. We propose that this facility, namely, to increase metal binding from the terminally-determined beads to the bridged clusters, allows for both delivery of essential metal to apometalloenzymes and allows for the domain specificity previously reported in many papers.

The question, therefore, that we address in this review concerns the ramification of the equilibrium structure prior to nominal metal saturation. Significantly, the advent of ESI-mass spectrometry has allowed determination of the exact speciation during the stepwise metallation.⁴²⁻⁴³ The ESI-MS data showed that stepwise metallation of MT proceeds not in single steps with a single increase in the metal status, but via a distribution of metallated species. As a consequence, the CD and emission spectroscopic data from our group mentioned above, are always an average of many species until the end of the titration when metal ions saturate all available binding sites. However, because of the similarity in the chromophores it has been very difficult to near impossible to determine the structures of the partially metallated species as the metallation reaction proceeds. An example of the value of the ESI-MS data is also found in the studies of the effect excess metal ions, such as cadmium^{30, 44}, where the combination of ESI-MS data and ¹¹³Cd NMR spectra showed the collapse of the typical two-domain structure into one 'super'-cluster took place.

Our goal with this review is to stimulate further studies into both the pre- and post-cluster structures of MT. Both are critical to the metallation chemistry of MT. The single domain concept described in this review is based on experimental work from mammalian MTs, but we recognize that in many of the other classes of MT there may be sequences that lend themselves to single domain formation, for example the plant MTs and the type 4 wheat MTs^{5, 15, 45-47}. It is outside the scope of this current review to discuss those structures, but we look forward to such a discussion in the future. We maintain that understanding the early stages of the metallation of MT prior to the cluster formation that occurs when the protein becomes saturated with metals challenges the conventional wisdom but that challenge will lead to a greater understanding of the formidable metal-based chemistry of the metallothioneins in general. We must note that while we describe here solely *in vitro* studies these might well involve species not necessarily formed *in vivo*. However, until instrumental techniques are developed to allow for the fast and sensitive detection of the complexes formed *in vivo*, the complexes discovered and characterized *in vitro* must be used as guides to the *in vivo* chemistry. Regardless, the usual inorganic

chemistry will govern complex formation between the thiols of the cysteines of the metallothioneins and the Cu⁺, Zn²⁺ and Cd²⁺ metals.

1.1 Mammalian Metallothioneins

Mammalian MTs are the most well studied member of the MT family and comprises 20 cysteine residues that act when saturated with 7 divalent metals to encapsulate two metal-thiolate clusters using a combination of bridging and terminal thiolates from the cysteinyl residues (Figure 1). We note to be clear, that when we use just "MT" in this review, we intend the meaning of mammalian MTs - commonly the series of human MTs and to avoid a complexity of nomenclature we refer the reader to the cited papers for the exact isoform used if we are not explicit. The N-terminal β-domain with 9 cysteine residues is capable of binding 3 Cd²⁺ or Zn²⁺, or 6 Cu⁺ and the C-terminal α-domain with 11 cysteine residues capable of binding 4 Cd²⁺ or Zn²⁺, or 6 Cu⁺. The two separate domains form a dumb-bell-like structure in the crystal first described from analysis of the X-ray diffraction data from rat liver MT-2^{21, 48}. Formation of the two metal-thiolate clusters has been generally proposed to take place in such a way as to allow for different types of metals to be selectively isolated into each domain⁴⁹⁻⁵⁰. By selective we mean that the protein is capable of discriminately allocating different types of metal ions into one of its two domains. For example, early NMR studies of MT were analyzed in terms of preferential binding of Zn²⁺ and Cd²⁺, to the α-domain while the β-domain preferentially binds Cu⁺. This selectivity has been proposed to allow for MT to take part in the homeostasis of a number of metal ions, while simultaneously isolating their respective chemistries^{18, 22, 51}.

There are four subfamilies of mammalian MTs that have been proposed to exhibit specific roles: MT-1 and MT-2, in the liver and kidneys, are induced by a number of stimuli including metal ions, glucocorticoids, cytokines and oxidative stress¹¹, MT-3 is primarily found in the central nervous system⁵², and MT-4, is found in certain stratified squamous epithelial tissues⁵³⁻⁵⁴. A number of stimuli can induce expression of both MT-1 and MT-2, while MT-3 and MT-4 are constitutively expressed⁵⁵⁻⁵⁶. Presumably, differences in expression are a consequence of the very different and specific roles of both MT-3 and MT-4. To support this proposal MT-3 is thought to be intimately involved in neurologically relevant Cu⁺ ion chemistry⁵⁷⁻⁵⁸ and disruption of the natural expression of MT-3, through ectopic expression in mice, has been shown to cause pancreatic acinar cell necrosis and death⁵⁹.

The several mammalian isoforms of MT have been shown to bind a remarkably wide range of metals *in vitro* including: Zn²⁺, Cd²⁺, Hg²⁺, Cu⁺, Ag⁺, Au⁺, Pt²⁺, Fe²⁺, As³⁺, Bi³⁺ and Tc^{5+ 27, 32, 34, 60-62}. We should point out that while many of the *in vitro* metallation studies have been carried out starting with the apo-protein, *in vivo*, metal substitution will also take place, especially with the replacement of Zn²⁺ by Cd²⁺ and Cu⁺. The beaded structure proposed for Zn-metallation will facilitate the protection of the cysteinyl thiols by binding as soon as the emerging peptide includes three or four cysteines³⁵. The lack of significant conventional secondary structure of the apo-MT has greatly complicated structural studies⁷⁻⁹. To improve understanding, a number of computational studies have demonstrated the presence

of a significant hydrogen bonding network in apo-MT-1⁶³⁻⁶⁵. It is thought that this network effectively stabilizes a more globular structure, where all cysteine residues are outwardly facing. This structure would then allow initial formation of the metal-thiolate bonds by facilitating interaction between the metal ions and cysteine residues. New data have shown that the structure of apo-MT-1 may be more globular than previously thought with significant similarities between itself and holo-MT^{64, 66}.

Further complicating the metallation studies of apo-hMT-1 by Zn²⁺, where Zn-MT is the dominant form found in mammals⁶⁷, is that the Zn²⁺ is essentially spectroscopically silent, requiring metal-ion substitution in order to be studied by many of the traditional metalloprotein techniques (UV absorption, CD and NMR spectroscopies). Because of this requirement, cadmium has been extensively used as a structural probe for zinc metallation³. There are several physical properties that make cadmium an ideal structural probe. Firstly, cadmium is isomorphous with zinc and is often shown to be isostructural, although ligand preferences are different. In the case of sulfur, however, the replacement of zinc by cadmium in MT has been commonplace. NMR spectroscopic studies have determined that Zn₇- and Cd₇-MT-2 have almost identical molecular architectures⁶⁸⁻⁶⁹. Secondly, the ligand-to-metal charge transfer associated with the cadmium-cysteinyli-thiolate bonds is red shifted (~250 nm), when compared to zinc-cysteinyli thiolate bonds (~230 nm), which makes it significantly easier to monitor changes in the metal (now cadmium) binding site using both UV absorption and CD spectroscopies²⁵. Finally, cadmium has a significantly greater affinity than zinc for the thiolate ligand, and this effectively enhances the stability of Cd-MT compared to Zn-MT, greatly increasing the binding constant, K_F. This property also contributes to a much greater resistance to aerial oxidation even when exposed to trace amounts of oxygen⁷⁰⁻⁷². However, the greater covalency of Cd²⁺ can significantly change the metal binding properties to the thiolate ligands of the cysteine residues in a manner not currently discussed for MT.

Cadmium metallation has been very informative in assisting in determining the zinc metallation chemistry of hMTs, however the advancement of electrospray ionization mass spectrometry (ESI-MS) has allowed the direct analysis of the metallation steps for Zn-MTs^{40, 42-43}. ESI-MS is a remarkably powerful technique and we will discuss its vital role in providing hitherto unobtainable data for the general case of the metallation of metallothioneins in greater detail later. Briefly, a major facet in the power of this technique is its facility for simultaneously determining the number, the identity of metal ions bound to a protein and the effect of the metallation has on the conformation of the protein through an analysis of changes to the charge state³⁸ profile of the protein. This technique, in particular, has provided a wealth of information on the early stages of the metallation of MT by Zn²⁺ and Cd²⁺, as well as by As³⁺ and Bi³⁺^{32-36, 39, 62, 73-74}. Important aspects of MT chemistry that are currently under investigation include specific details of the stepwise metallation as it proceeds along a pathway from the metal free (apo-) MT to the fully metallated (holo-) MT and the studies of structure of the apo-metallothionein and partially-metallated species.

1.2 Non Mammalian Metallothioneins

Proteins with the defining characteristics of MT have been isolated from a wide array of sources¹¹. These proteins have each

evolved unique metal-binding sites and domains in order to bind different metals (Cu⁺ and Zn²⁺) with different stoichiometries. We will briefly touch on four different MTs from the following sources: *Lumbricus rubellus* (earthworm), *Fucus vesiculosus* (seaweed), *Synechococcus* PCC 7942 (cyanobacteria) and *Triticum aestivum* (bread wheat). Each is significantly different from the mammalian form of the protein with its 20 cysteine residues distributed into both an N-terminal β-domain and a C-terminal α-domain composed of 9 and 11 cysteine residues, respectively.

The MTs found in earthworm (*Lumbricus rubellus*) are of considerable interest, because their presence can be directly related to both soil quality and fertility. Interestingly, earthworms native to the Rudry mining sites (South Glamorgan, Wales) were capable of tolerating cadmium soil content of 604 μg Cd/g dry weight and were capable of bioaccumulating cadmium to 1213 μg Cd/g dry weight⁷⁵. The ability of earthworms to act as a bioindicator and bioaccumulator of soil cadmium content has created significant research interest into their use as both markers of the health of the soil, as well as the potential for their use in land reclamation. In either case, an understanding of the metabolic uptake and subsequent distribution of cadmium in the organism is essential for their future use⁷⁶⁻⁷⁷.

Three distinct worm MT isoforms (wMT-1, 2 and 3) have been isolated from *Lumbricus rubellus*^{75, 78}. Both wMT-1 and 2 have a total of 20 cysteine residues. Interestingly, a combination of spectroscopic and spectrometric studies of wMT-2 have suggested the order of the two domains is reversed – that is an N-terminal α-domain and a C-terminal β-domain both of which act to encapsulate 7 Cd²⁺ ions⁷⁹. This reverse has also been observed in the sea urchin MTA isoform and may have an as yet unknown function⁸⁰.

It has been suggested that each of the wMT isoforms have a specific function in the organism⁷⁸. In the case of wMT-2, induction studies have shown that it is strongly expressed upon cadmium exposure. wMT-1 has also been suggested to be involved in the homeostasis of essential Zn²⁺ and Cu⁺ owing to its enhanced ability to donate essential metals. Finally, wMT-3 is highly abundant and functionally active during embryonic development. Taken together, these results support the view that different isoforms of MT have specialized functions.

Seaweed MTs, including *Fucus vesiculosus*, have many of the attributes that make them ideal bioindicators for marine ecosystems, including resistance to heavy metal pollution, the ability to bioaccumulate metal-ions (namely zinc and copper), as well as their widespread distribution⁸¹. A single *F. vesiculosus* MT protein, fMT, was isolated from the cDNA library of macroalgae adapted to prolonged exposure to copper salts. The sequence of fMT was shown to contain 16 cysteine residues: an N-terminal, 9 cysteine, β-domain and a C-terminal, 7 cysteine, 'γ'-domain separated by a linker-region of 14 amino acids. This linker region is of significant interest, because it is of intermediate length when compared to the small linkers found in vertebrate MTs (3 residues) and the longer linkers found in many plants (~40 residues). The length of the linker may be helpful in modulating the interactions between each domain, with smaller linkers, such as those found in the mammalian MTs, promoting

some domain-domain interactions, and the longer domains further isolating the two domains, and their corresponding chemistries, from each other.

A significant body of both spectroscopic and spectrometric work has contributed to our current knowledge of the metallation chemistry of *f*MT⁸². *f*MT is capable of binding 6 Cd²⁺ or Zn²⁺ ions with its 16 cysteine residues. In addition, acid induced demetallation has suggested that 3 Cd²⁺ or Zn²⁺ ions were located in both the β - and γ -domains forming M₃S₉ and M₃S₇ clusters, where M corresponds to either Cd²⁺ or Zn²⁺.

ESI-MS kinetic analysis of arsenic binding to *f*MT has shown that the β - and γ -domains bind 3 and 2 As³⁺ ions, respectively, in a series of sequential reactions⁷⁴. The binding of As³⁺ to *f*MT occurs at a pH of 3.5 indicating greater affinity for thiols than either Zn²⁺ or Cd²⁺. The kinetic results demonstrate that both domains act as effectively isolated units because the rate constants do not appear to follow a single, statistically driven trend. This conclusion is in stark contrast to As³⁺ binding to human MT where the presence of both domains acts to enhance the binding rate that follows a single, statistically-driven trend³²⁻³⁴. This difference has been attributed primarily to the extended length of the linker region of *f*MT (14 residues), when compared with the linkers in the recombinant human MT-1 (6 residues) and native human MT-2a (3 residues).

The ability of *f*MT to strongly bind arsenic has led to the recent modification of an *E. coli* strain to express *f*MT leading to the rapid removal of arsenic (as both As³⁺ and As⁵⁺) from contaminated water⁸³. This system was highly selective for arsenic, even in the presence of equimolar concentrations of zinc, lead, or cadmium. Taken together, these results show great promise for future use of *f*MT in both the reclamation of aquatic environments, as well as the purification of potable water.

The cyanobacterium *Synechococcus* PCC 7942 is also known to express a relatively small (56 residue) MT-like protein, SmtA⁸⁴. This protein is required for normal zinc tolerance and is synthesized upon exposure to elevated concentrations of metal ions, specifically zinc, cadmium and copper. Unlike the MT proteins mentioned above, which coordinate metal ions through only cysteine residues, SmtA coordinates four Zn²⁺/Cd²⁺ ions using 9 cysteine and 2 histidine residues. Further, unlike the MT species that exist as two distinct metal-thiolate clusters when saturated with metals, NMR structural analysis has conclusively shown that this protein exists as a single M₄Cys₉His₂ domain, where M corresponds to either Zn²⁺ or Cd²⁺⁸⁵.

The SmtA cluster, M₄Cys₉His₂, is structurally similar to the α -domain of mammalian MT, M₄Cys₁₁ (Figure 1). However, unlike the α -domain of mammalian MT, where all four Zn²⁺ or Cd²⁺ ions are bound to cysteine residues, 2 of the 4 metal ions in SmtA are each coordinated to 1 histidine and 3 cysteine residues, while the remaining 2 are coordinated to exactly 4 cysteine residues. Therefore, SmtA is in its detail, quite unlike a typical mammalian metallothionein. Interestingly, mutational studies have shown that substitution of the histidine residues found in SmtA, with the more conventional cysteine residues, significantly alters both the overall fold of the protein, and as well the metal-binding dynamics⁸⁶.

One of the two Zn₁Cys₄ binding sites (site A) has been shown to have significant similarity in arrangement and orientation,

including the associated α -helix and β -strands, with the C-terminal zinc finger of the eukaryotic DNA binding protein GATA-1 and it is this zinc-finger motif that enhances selectivity for Zn²⁺ ions, as opposed to Cd²⁺ ions⁸⁷. This Zn²⁺ ion has been shown to be inert to metal exchange with other Zn²⁺ ions as monitored through very high resolution ESI-MS⁸⁸, as well as towards loss to competitive chelators, such as 16 molar equivalents of EDTA, forming the long-lived intermediate Zn₁-SmtA. Importantly, the presence of this final Zn²⁺ ion allows the overall structure of the protein to be maintained and may aid its recognition by apo-enzymes.

Plant MTs are characterized by their relatively large size (~7-8 kDa) compared to vertebrate MT (~6 kDa), greater sequence diversity and most importantly the presence of a long, cysteine free, linker region (~40 residues) separating two cysteine rich regions⁴⁵. While the exact function of this linker is unknown, it is interesting to note that aromatic amino acids, lacking in mammalian MTs, are found here. The exact functions of plant MTs have been studied to a lesser extent than mammalian forms. Nevertheless, plant MTs have been suggested to be involved in both metal ion homeostasis and metal-ion detoxification. However, in the case of metal-ion detoxification plants are capable of enzymatically synthesizing phytochelatin in response to toxic metals, such as cadmium, and thus metallothioneins may be of less importance for this role in plants than in mammals⁵. It is this reliance on phytochelatin that may have allowed plant MTs a greater ability to differentiate from the previously mentioned MT species.

The only available three dimensional structure of plant MTs is of E_c-1 from *Triticum aestivum* (common bread wheat). E_c-1 are strongly expressed during the earliest stages of germination, where they account for between 20-25% of the total cysteines incorporated into nascent proteins. The protein contains three cysteine rich regions: an N-terminal region with 6 cysteine residues, a C-terminal region with 5 cysteine residues, and finally a central region containing both 6 cysteine residues and 2 histidine residues. From these metal-binding amino acids, E_c-1 is capable of binding Zn²⁺ ions into two distinct domains: a C-terminal Zn₂Cys₆ ' γ '-domain and an N-terminal Zn₃Cys₉ β -domain, as well as a singular Zn₁Cys₂His₂ binding site⁴⁶⁻⁴⁷. While the presence of coordinating histidine residues in MT proteins has been previously reported (see above), the presence of a mononuclear binding site is unprecedented and may have significant consequences for the cellular functions of the protein.

2. Challenging Conventional Wisdom

Many proposals for the mechanism of metallation of MTs have been put forward. Initial studies, specifically using NMR spectroscopy, advocated a singularly cooperative mechanism. This proposal argued that the binding of the n+1 substrate, or metal ion in the case of MT, (K_{n+1}) will have greater affinity for the protein than that of the n substrate (K_n), such that K_{n+1} > K_n. To summarise, only the substrate-free or fully-bound protein would be predicted to exist and partially-metallated intermediates would be unstable and, therefore, unlikely to take part in cellular chemistry. A well known example of cooperativity in Nature is the coordination of four oxygen molecules to hemoglobin⁸⁹. In

this system, as each oxygen molecule binds the affinity for further oxygenation increases. As such, the affinity of hemoglobin for the fourth and final oxygen molecule will be greater than for either of the three previous ones ($K_{4th-O_2} > K_{3rd-O_2} > K_{2nd-O_2} > K_{1st-O_2}$). Consequently, one would expect there to exist, at a given partial pressure of oxygen, a mixture of oxygen-free and fully-oxygenated hemoglobin with few, if any, intermediates present.

In MTs, a cooperative and domain specific metallation mechanism, where addition of up to 4 equivalents of Cd^{2+} are exclusively bound by the α -domain and the next 3 equivalents are bound by the β -domain, was the long held metallation model for Zn^{2+} and Cd^{2+} . In this model, as we show below, there would be only very low concentrations of partially metallated species. However, the advent of ESI-mass spectrometry has allowed the simultaneous visualization of the multiple, partially-metallated species. Indeed, using ESI-MS techniques, a number of partially metallated states were observed and, as it is shown in section 3.1, the metallation of rhMT-1 under specific pH and ionic strength conditions is in fact noncooperative for Zn^{2+} , Cd^{2+} and As^{3+} . Unlike many spectroscopic techniques that provide a mass average, in other words a weighted average of the chromophoric signature of the differently metallated Zn- or Cd-thiolate species, the high resolution of ESI-MS differentiates readily between both different numbers of the same metal bound to the apo-protein (for example, clearly and unambiguously between apo-MT and Zn_1 -MT then Zn_2 -MT and Zn_3 -MT, etc.) and also between mixtures of metals as is the case for Zn^{2+} and Cd^{2+} (for example, between apo-MT and Zn_1 -MT and Cd_1 -MT and then Zn_1 - Cd_1 -MT).

2.1 ESI-mass spectrometry of metallothioneins

Electrospray ionization mass spectrometry is an informative technique that provides excellent and significant information about the early stages of metallation of metalloproteins. These data were previously considered difficult (if not impossible) to obtain by conventional spectroscopic means. ESI-MS achieves this information by measuring the mass-to-charge ratio (m/z) of proteins. From an analysis of either the isotopic distribution of a given charge state, or through the deconvolution of a series of related charge states the mass of the protein can be calculated. In the case of hrMT 1a, binding of metal ions to the protein, for example Cd^{2+} or Zn^{2+} , results in an increase in the m/z that is directly related to the mass of the bound metal^{36, 39}. In this way, we are now able to monitor the relative distribution of a mixture of differently metallated species. Prior to the wide-spread use of this technique, MT was often assumed to be homogeneously metallated, meaning, for example, that the addition of 4 equivalents of Zn^{2+} would exclusively form Zn_4 -MT-1. In reality, the ESI-MS data show very clearly that when 4 eq. of Zn^{2+} are added to a solution a mixture of Zn_3 -, Zn_4 -, Zn_5 - and Zn_6 -MT-1 coexist with Zn_4 -MT-1 as the most dominant species present³⁶. A brief description of the technique, followed by how data is interpreted, will allow for a better understanding of its usefulness in studying the complex metal binding properties of MTs. It should be noted at this time that not all complexes that are detected by ESI-MS may be stable *in vivo*.

In ESI-MS, a sample is introduced in solution, under atmospheric pressure, into the tip of the electrospray capillary. This tip is electrically charged to several thousand volts and allows for accumulation of positive or negative charge in the solution. Enrichment of the tip with positive or negative ions leads to the formation of a Taylor cone, which ejects small positively or negatively charged droplets. Solvent evaporation decreases the radius of the droplet, while the charge remains constant. When the surface tension of a droplet is overcome by Coulombic forces, due to the nearness of the charged ions, fission of the droplet occurs. Evaporation-fission events repeat until very small charged droplets are produced. Eventual formation of the multiply charged protein is thought to occur via the charged residue model (CRM)⁹⁰⁻⁹¹. The CRM mechanism of gas phase ion formation states that the small highly charged droplet will evaporate to dryness leaving any unpaired ions as adducts to the protein. Since each droplet will have varying numbers of unpaired ions, a distribution of mass-to-charge ratios will be observed. This charge state distribution is related to the surface area of (and, therefore, the volume occupied by) the protein. As such, any alterations in the size of the protein, either through metallation, folding, or denaturation will invariably lead to changes in the charge state distribution manifold. These changes will then lead to a decrease (in the case of folding) or increase (in the case of unfolding) of the centre of the charge state manifold observed in the ESI-mass spectrum. Charged proteins are then separated by differences in their respective m/z ratios allowing detection of species even with very similar m/z values.

The overall shape of the charge state envelope, that is the relative abundance of each charge state, can, therefore, be used to predict changes to the overall fold of the protein based following a chemical stimulus. Proteins, owing to their relatively large size and dynamic properties, will be able to accept a range of charges that depend on a combination of the overall volume of space occupied, as well as the number of exposed basic sites. As a general rule, unfolded proteins occupy a larger volume than their folded counterparts and will have charge state envelopes with a greater maximum charge (larger maximum z), and a greater total number of charge states (greater range of z 's). For example, when comparing the charge state envelopes of apo-MT-1 and Cd_7 -MT-1 (Figure 2), we immediately see apo-MT-1 (Figure 2A) has charge states that range from +8 to +5, while Cd_7 -MT-1 (Figure 2B) has charge states that range from +7 to +5. In the complete metallation of MT-1, not only did the maximum supportable charge state decrease when apo-MT was converted into Cd_7 -MT-1 (+8 vs. +7), but also the total number of supportable charge states decreased (4 vs. 3). These results show that the fully metallated, Cd_7 -MT-1, protein occupies a smaller volume than the unfolded protein. Increases in the manifold maximum are far more pronounced when the protein denatures at very low pH values.⁶⁶

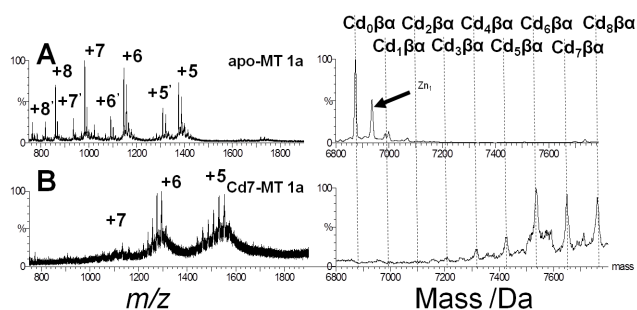


Figure 2. ESI mass spectra recorded during the titration of MT with Cd^{2+} . (A) Metal-free (apo)-MT-1 at 0 eq. Cd^{2+} added to solution and (B) $\text{Cd}_{6/7/8}$ -MT-1 at 7.3 eq. Cd^{2+} added to solution. Charge states +5' to +8' correspond to a less prevalent truncated species. Modified from Sutherland and Stillman³⁹ with permission from Elsevier (2008).

The ESI-MS technique allows for the introduction of samples in aqueous solution, at physiological pH, and allows one to quantify the sample composition. Folding experiments can be conducted, in which the charge state distribution can be directly related to changes in sample conditions, such as pH or metal added, and changes in metallation status can be monitored through mass changes. By knowing the concentration of protein, from spectroscopic techniques, accurate quantification is possible by a comparison of the deconvoluted peaks. This, however, assumes that all species in solution ionize at the same rate, and may not always be true. Using this technique, experiments have analyzed the mechanism of metallation of MT, the kinetics of metal binding to MT, as well as metal-ion competition experiments, which when modelled provide the formation constants of MT. These results will be discussed in detail, later in the text. Perhaps the most exciting experiments possible by ESI-MS techniques involve both the time- and temperature-dependence of the metallation reaction. The studies by Ngu and Stillman and co-workers have demonstrated a remarkable facility of the ESI-MS technique for proteins.³¹⁻³⁴ Together, the use of ESI-MS techniques in equilibrium studies and kinetic studies has provided a new and powerful tool with which to determine stepwise metallation parameters.

3. Mechanism of MT Metallation

The mechanism of metallation and the possible stable partially-metallated states profoundly impact our understanding of the functions of MT. The metallation status directly relates to the ability of MTs to play a role in detoxifying toxic metals, maintaining metal ion homeostasis, and acting as a protective agent against oxidative stress. Studies since the 1970s have alluded to a cooperative mechanism of metallation, in which the binding of one metal facilitates the binding of the next. However, recent experimental data, specifically ESI-mass spectral studies, have shown that metallation can occur in a noncooperative manner, where each metallation event occurs independently of the others and does not involve the initial formation of metal-thiolate clusters.^{32, 34, 39-40, 73}

3.1 Noncooperative mechanism of metallation

In a noncooperative metallation reaction, the binding of a metal ion leads to a reduction in the number of available metal-binding sites. For example, in the case of As_6 -MT-1 (see below for greater detail), the first As^{3+} ion binds to apo-MT-1 to form As_1 -MT-1 and has six available sites to form this complex; however, binding of the second As^{3+} ion to As_1 -MT-1 forming As_2 -MT-1 has only five available sites (a total reduction of one available binding site)³²⁻³⁴. From this reduction in the number of available binding sites, we can experimentally observe a reduction in the binding kinetics, and consequently, the association constant. The affinity of a metal ion for MT is statistically related to the number of available binding sites and the dominant metallation state will be related to the number of metal ions in solution. Further, this means that partially metallated forms of MT are stable and may be relevant to the cellular functions of an organism⁹². Consequently, studies reporting the coexistence of metal free MT, both oxidized and reduced, with metallated MT, can be rationalized as normal and expected properties of the protein⁹³.

Several spectroscopic studies have suggested a noncooperative mechanism of metallation including CD and EPR spectroscopy. In the first case, rabbit liver MT-1 was titrated with Cd^{2+} and a concomitant increase in the intensity of a broad monophasic peak (~250 nm) associated with the ligand-to-metal charge transfer was observed⁹⁴. Past the 3 molar equivalents of Cd^{2+} added point, there is a changeover from a broad monophasic peak to a biphasic CD characterized by positive ellipticity at 260 nm, a crossover point at 250 nm, and negative ellipticity at 240 nm. This biphasic spectrum was interpreted as resulting from the occurrence of clustering, and the subsequent increase in symmetry. Further, the transition from a broad monophasic peak to a biphasic peak suggests that during early metallation, when the number of cadmium atoms is limiting and there is an abundance of thiolate ligands, isolated Cd_1Cys_4 units form. Only when terminal thiolate coordination is exhausted does bridging occur.

Further evidence for noncooperative metallation can be seen through a titration of rabbit liver MT-1 with Co^{2+} as monitored by EPR spectroscopy⁹⁵⁻⁹⁶. EPR spectroscopy is unique in that it measures the number of unpaired electrons. The EPR signal ($g_x = 5.9$ measured at 4 K) increased linearly up to, and including, 4 equivalents of Co^{2+} . However, a linear decrease in signal intensity is observed past 4 molar equivalents of Co^{2+} . The authors argue that this decrease is brought about by antiferromagnetic coupling of neighbouring Co^{2+} ions. The significant consequence of these results is that up until 4 molar equivalents of Co^{2+} has been added, nonbridging Co_1Cys_4 clusters must dominate the spectrum, after which bridging interactions lead to the more traditional 3 metal and 4 metal clusters of MT.

A number of recent mass spectrometric titrations have argued for a noncooperative mechanism of metallation for Cd^{2+} , Zn^{2+} , As^{3+} and Bi^{3+} binding to human apo-MT-1^{32, 34, 36, 39, 62}, and its isolated domains, as well as Cd^{2+} and Zn^{2+} binding to brain specific human MT-3⁴⁰. At this time it is unclear if the mechanism of metallation of MT is isoform specific, that is do MT-1 and MT-3 bind metal ions in a noncooperative manner,

while MT-2 binds metal ions in a cooperative fashion? Further investigation of the metallation properties of hMT-2 will be necessary in order to resolve this dilemma and determine the specific, cellular-relevant, conditions that enhance both the noncooperative and cooperative mechanisms.

3.2 ESI-mass spectral titration of apo-MT with Zn^{2+}

We will at this point describe in detail, the metallation of MT-1 with Zn^{2+} . This experiment demonstrates the resolving power of ESI-MS for differently metallated species and how this information can aid in solving mechanistic questions concerning the mechanism involved. Analysis of these data led to the conclusions first referred to in section 1.0.³⁶ The mass spectral data recorded during the titration of apo- β -rhMT-1 with Zn^{2+} at pH 9.5 and the corresponding deconvoluted spectra are shown in Figure 3 (A-E)³⁶.

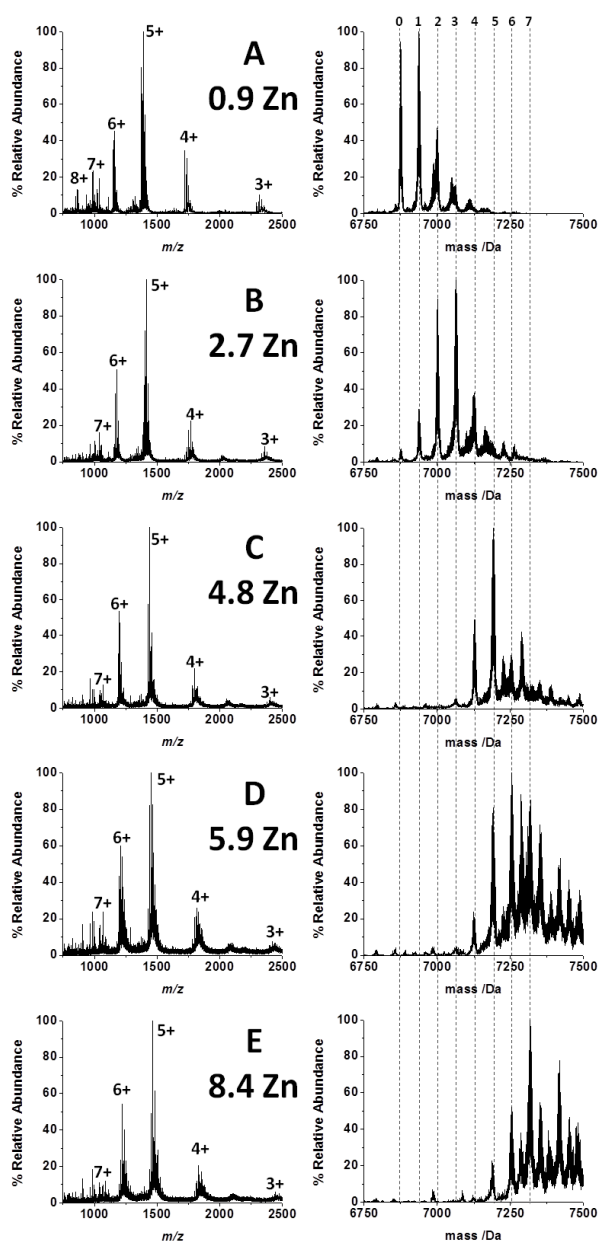


Figure 3. ESI mass spectra recorded during the titration of apo- β -rhMT-1 with $ZnSO_4$. Spectral changes were recorded as aliquots of Zn^{2+} were titrated into solution. Dotted lines follow metal binding status. Mass spectral charge states of β -rhMT (left) and their deconvoluted counterparts (right) were recorded at Zn^{2+} molar equivalents of 0.9, 2.7, 4.8, 5.9, and 8.4. The peak between Zn_6 - and Zn_7 - β -rhMT at 5.9 equivalents of Zn^{2+} has been identified as Zn_6 - β -rhMT with a chloride adduct bound. Metallation in excess of Zn_7 - β -rhMT is result of nonspecific adducts. Reprinted with permission from Sutherland *et al.*³⁶ copyright (2012) American Chemical Society.

As expected for a noncooperative system, stepwise metallation of apo- β -rhMT-1 leads to the formation of partially metallated species (from Zn_1 to Zn_6) at substoichiometric equivalents ($Zn:\beta < 7 Zn^{2+}$). The endpoint of the titration occurs after 7 equivalents of Zn^{2+} have been added to the solution and is likely the result of slight errors in the estimation of the apo-protein concentrations, as well as the formation of trace amounts of competitive $Zn(OH)_2$ due to the alkaline pH of the solution.

In each step of the titration, the dominant metallation state is the direct result of the number of equivalents of Zn^{2+} added to solution. For example at 0.9 equivalents of Zn^{2+} , the dominant metallation states are apo- and Zn_1 - β -rhMT, while at 2.7 equivalents of Zn^{2+} , the dominant metallation states are Zn_2 - and Zn_3 - β -rhMT. What is important is that there exist a number of partially-metallated species that have as their weighted average the stoichiometric amount of zinc added.

Apo- β -rhMT-1 exhibits a charge state profile that ranges from 8+ to 3+. As Zn^{2+} coordinates to apo-MT-1, a significant reduction in the intensity of the 7+ charge state, as well as the disappearance of the 8+ charge state is observed. These changes to the charge state manifold suggest that the first metal ion must significantly restrict the motion of the protein, as well as reduce the volume it occupies. Beyond 2.7 eq. Zn^{2+} , there is very little change in the 6+, 5+, 4+ and 3+ charge state distribution indicating that further metallation does not substantially increase the folding of the protein.

One aspect of the titration is the stability of Zn_5 - β -rhMT-1 (Figure 3C). At the 4.8 Zn^{2+} point in the titration, the spectra are significantly simplified with only Zn_5 - and $\sim 33\%$ Zn_4 - β -rhMT-1. This simplification in the number of species suggests that the association constant (K_F) of Zn_6 - β -rhMT-1 is significantly weaker than that of Zn_5 - β -rhMT-1 so that low metallation states must be exhausted before the formation of significant Zn_6 -MT-1. While the exact reason for the drop is uncertain at this time, we propose that at 5 equivalents of Zn^{2+} each of the 5 Zn^{2+} ions is coordinated to 4 terminal cysteine residues and that binding of the 6th Zn^{2+} ion requires a rearrangement of these residues to form the first part of the expected 2-domain structure. The change in binding affinity has also been previously discussed by Krezel and Maret⁷⁰. As mentioned above, a number of studies using a range of techniques, including ^{113}Cd -NMR, Co-EPR and CD spectroscopies, to monitor metallation titrations have concluded that the initial metallation of MT must occur through exclusively terminal cysteine residues, after which cluster formation leads to bridging interactions^{19-20, 95-97}. Simply put, the 5 Zn^{2+} are coordinated terminally using all 20 cysteine thiols before

clustering takes place – this being the typical property of a 5-metal binding-site, which is a single metal binding domain. These experimental results were interpreted as showing that the well-known two-domain cluster-based structure does not begin to form until the 6th Zn²⁺ is bound.

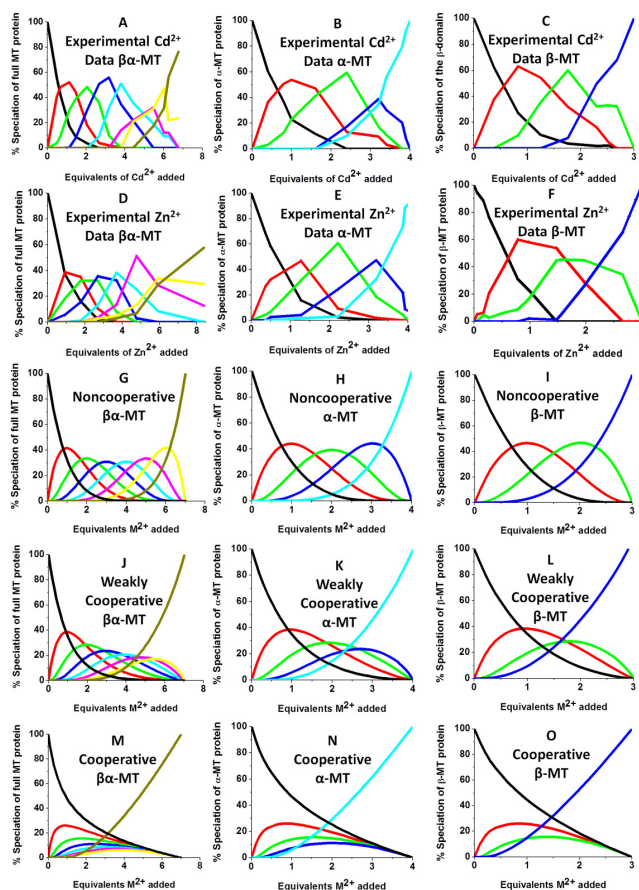


Figure 4. Experimental ESI-MS data and simulations of ESI-MS data for the metallation of MT and its isolated domains with Cd²⁺ and Zn²⁺. Models and experimental data showing Cd²⁺ speciation (A, B, C) and Zn²⁺ speciation (D, E, F) during metallation of the full MT protein, and the α - and β -domains. A noncooperative model (declining K_a 's) of ESI-MS data based upon a series of linearly decreasing association constants (G, H, I). A weakly cooperative model (equal K_a 's) of ESI-MS data based upon a series of equal association constants (J, K, L). A strongly cooperative model (increasing K_a 's) of ESI-MS data based upon a series of linearly increasing association constants (M, N, O). Each line corresponds to a different metallation state: Zn₀ (—●—), Zn₁ (—■—), Zn₂ (—▲—), Zn₃ (—▼—), Zn₄ (—◆—), Zn₅ (—☆—), Zn₆ (—◇—) and Zn₇ (—◇—). We note that the values of the K 's used in the modelling were chosen to illustrate the binding mechanism and are not representative of binding in any protein. Reproduced from ref³⁷ with permission from Elsevier (2012).

We have modelled the experimental mass spectral data (Figure 4), as well as the expected distribution of partially metallated species for the three mechanistic extremes: (i) a noncooperative mechanism, (ii) a weakly cooperative mechanism, and (iii) a cooperative mechanism. The simulations were plotted to show metal ion speciation as a function of the equivalents of divalent

metals (Zn²⁺ or Cd²⁺) added to a solution of apo-MT-1 (either as the isolated fragments or the full protein)³⁷.

In the case of a noncooperative mechanism (Figure 4 G, H, I), we assume that the first five sites (terminal thiolate binding), as well as the final two (bridging thiolate) sites have a decreasing affinity for divalent metals; a decrease that is statistically controlled by the number of available binding sites. The observed affinity of metals for the metal-saturated protein is a result of the summation of all the K 's for the available sites. For example, when comparing the affinity of apo-MT-1 to Zn₆-MT-1, the occupation of 6 binding sites reduces the affinity of the latter for the seventh metal ion to 1/7 that of the K for the apo-protein to bind the 1st metal.

In the case of a weakly cooperative system (Figure 4 J, K, L), we assume that the sum of available binding sites will always have equal affinity for divalent metals, regardless of current metal-ion occupancy. We describe this situation as weakly cooperative, because the association constants for the full MT-1 protein statistically decrease based on the number of available metal-binding sites. However, this statistical decrease is compensated for by an increase in the affinity of each individual binding site. If this model were correct, then the only thermodynamic basis for it would be an increase in the hydrogen bonding network as a function of increased metallation.

In the final case, strongly cooperative metallation (Figure 4 M, N, O) assumes that binding of each metal ion leads to a linear increase in MT for further metallation. As such, when comparing the association constants for apo-MT-1 and Zn₆-MT-1, the latter has an affinity that is 7-times greater than the former.

As one would intuitively predict, the modelling data for both the cooperative and weakly cooperative systems lead to the early formation of the fully metallated Zn₇-MT-1 complex (dominates spectra at 3 and 5 equivalents for the cooperative and weakly cooperative systems, respectively). In the case of a noncooperative mechanism of metallation, the fully metallated species dominates the spectra after 6 equivalents of Zn²⁺ have been added to the solution. Another significant difference between the three mechanisms is in the relative abundances of each intermediate. In the noncooperative system all intermediates are of roughly equal intensity (at their maxima), while in both the cooperative and weakly cooperative systems the intensities of the respective partially-metallated intermediates (at their maxima) vary and are not nearly as abundant as in the noncooperative system.

By comparing these three models with the experimental data (Figure 4), it is clear that apo-hMT-1 metallates in a noncooperative manner. The experimental data show that the abundance of each species is directly related to the amount of Zn²⁺ added to solution. In addition, the intensity of each intermediate is of roughly equal intensity to those of the theoretical noncooperative data. Further, the fully metallated Zn₇-MT-1 does not dominate the spectra until after 6 equivalents of Zn²⁺ have been added to solution, and even then there is still a significant amount of Zn₆-MT-1 remaining. To our knowledge this is the first time that the stepwise titration of any apo-MT with either Zn²⁺ or Cd²⁺ has been modelled for all three systems

(noncooperative, weakly cooperative, and strongly cooperative) and it is clear from the very similar shape that apo-hMT-1 metallates in a noncooperative fashion. We should note at this point that each of the twenty cysteinyl sulphurs will have a pKa of roughly 8. As such, the total charge of the protein may be significantly altered with the pH of the solution. The current experimental data described in this review were performed under slightly alkaline conditions, and at the present moment it is unclear whether acidification alters the mechanism of metallation. The presence of apo-MT in the kidneys of mammals is well documented^{3, 10}, and it is also known that humans are capable of acidify urine to pH values below 5 (acidic). Studies are currently underway to determine if there is a change in the mechanism when the solution is more acidic. These results will have homeostatic significance for the balance of metal ions in the different organ systems of the body. For example, metallation in the kidneys may occur at significantly lower pH values

3.3 Kinetics of MT metallation

The ESI-mass spectral studies referred to above show that both Zn^{2+} and Cd^{2+} bind to MT in a noncooperative manner to rhMT-1, one must keep in mind that these structures represent thermodynamic minima. Importantly, the kinetic analysis of metallation would provide new insight into the metallation properties of MT - specifically the importance of the initial single and subsequent two domain structure. Unfortunately, for further mechanistic work using kinetic analysis the binding of both Cd^{2+} and Zn^{2+} to apo-MT is complete within several milliseconds⁹⁸. To date, only the time-dependence and temperature-dependence of arsenic, which binds on the order of minutes, has been studied intensively by ESI-mass spectrometry^{31-34, 74}. Arsenic binds to apo-MT in a trigonal pyramidal fashion through terminal coordination of 3 cysteine residues. Unlike either Cd^{2+} or Zn^{2+} , which are known to form clustered structures involving shared ("bridged") thiolates, As^{3+} only binds to terminal cysteines. This makes As^{3+} an ideal model for studying the early stages of metallation prior to the formation of clusters; that is as an example of the single domain region.

The lack of clustering properties in As-MT provides a simplified picture of metallation, and is thus ideal for understanding the early stages of metallation, when metal ions are limiting and unable to form clusters. Of the four human MT isoforms available, only MT-1 has been studied in this manner³²⁻³⁴. In addition to human MT-1, As^{3+} binding to *Fucus vesiculosus* has also been reported⁷⁴. These studies of As^{3+} binding are likely to be a model for other metals because they definitively show the mechanism of metallation to be noncooperative and they also demonstrate metallation occurring as a series of sequential bimolecular reactions.

More significant, and related to our understanding of the mechanism before cluster formation takes place, analysis shows that the rate of metallation is directly dependent on the number of available binding sites, with the isolated β - and α -domains binding As^{3+} the slowest and the full MT-1 protein binding As^{3+} the fastest (Figure 5).

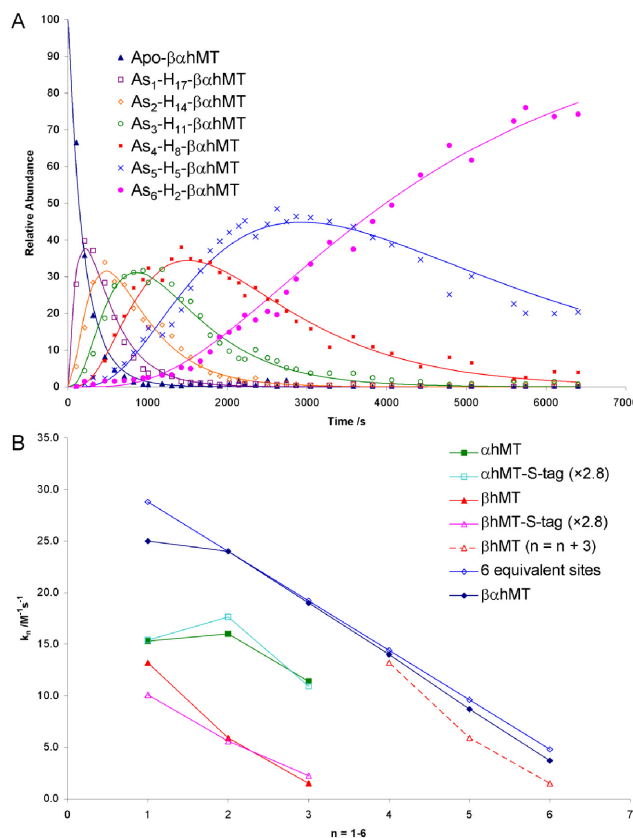


Figure 5. (A) Time-resolved ESI-MS relative abundances human apo- β - α -rhMT-1 and As_n -bound species ($n = 1-6$) following reaction with excess As^{3+} at 25 °C and pH 3.5. Human β α MT has the sequence shown in Figure 1 with 20 cys binding 6 As^{3+} leaving 2 cys free¹⁰⁶. The α -hMT and β -hMT fragments each bind 3 As^{3+} . The reaction was carried out with an As^{3+} : MT stoichiometric ratio of 11:1. The relative abundances of each of the species are shown as the data points on the graph. The lines were calculated by fitting all the data to a series of six, consecutive bimolecular reactions. (B) Comparison of the rate constants calculated from the time-resolved ESI-MS measurements for As^{3+} -metallation of α -rhMT-1-s-tag, β -rhMT-1-s-tag, the full protein β α -rhMT-1 and the trend in rate constant values for six equivalent sites where $k_1 = 28.8 \text{ M}^{-1}\text{s}^{-1}$. The dashed line represented rate constant data for the β -rhMT-1 redrawn with the value of n shifted by three illustrate the similarity of the rate constant trend for the final three As^{3+} binding to the β -rhMT-1. The protein used was recombinant human (rh) MT-1. Reprinted with permission from ref³² copyright (2008) American Chemical Society.

The report of the kinetics of As^{3+} binding to the genetically engineered triple domain $\alpha\alpha$ -hMT-1 with 33 cys and $\beta\beta$ -hMT-1 with 27 cys, confirmed that initial metallation is fastest in these two systems, and that rates decreased as more As^{3+} binds. The most important result with respect to metallation generally is that in every case studied, the last metal binds with the slowest rate and, therefore, the lowest affinity³³. Figure 5A shows the time resolution of the appearance and disappearance of the different As_n -MT-1 species. The data presented here show the time-resolved relative abundances of all the species measured

continuously up to 7,000 sec. The smooth lines correspond to a model that uses only the initial concentrations of the apo-MT and As^{3+} in a multivariate fit connecting a series of sequential, bimolecular reactions to the experimental data. Figure 5B clearly shows that the magnitude of the rate constants is directly dependent upon the number of available binding sites, where $n = 0 - 3$ for the isolated fragments and $n = 0 - 6$ for the two-domain $\beta\alpha$ -rhMT-1. The experiment was greatly extended by analyzing both temperature- and time-dependent ESI-MS data recorded during the metallation reaction. The close fit to each set of data, and the ability to simulate the As^{3+} distribution at a specific time with a known amount of protein, proved that the overall metallation reaction proceeded as a series of sequential, irreversible bimolecular reactions, where As^{3+} binds to 3 cysteine residues.

At equilibrium with substoichiometric As^{3+} equivalents, the stability of a number of partially-metallated As-MT-1 species further emphasized the noncooperative nature of the metallation of MT. There was concern that the use of the low pH (approximately 3.5) necessitated because the As^{3+} solutions were unstable above pH 3.5, meant that the binding was carried out at pH values that were too low to be biological relevant to humans. However, in 2010 our group reported that in fact the fully metallated As_6 - $\beta\alpha$ -rhMT-1 was stable at neutral pH and more critically, could transfer As^{3+} to both apo- α -rhMT-1 and apo- β -rhMT-1³¹ at neutral pH.

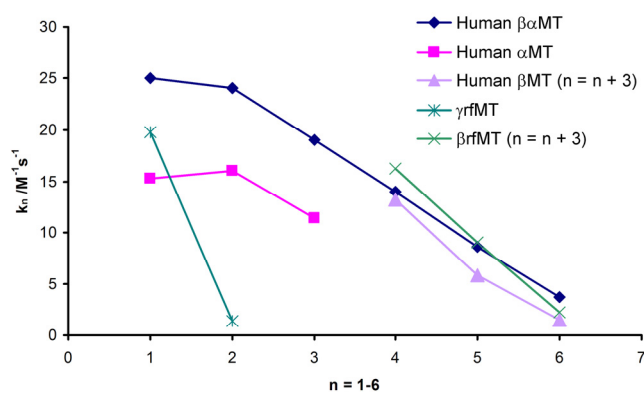


Figure 6. Comparison of the rate constants calculated from time-resolved ESI-MS measurements for As^{3+} metallation of α -rhMT, β -rhMT, $\beta\alpha$ -rhMT, γ -rfMT, and β -rfMT. The rate constant data for β -rhMT and β -rfMT were drawn with the value of n shifted by 3 to illustrate the similarity to the rate constant trend of the final three As^{3+} binding to $\beta\alpha$ -rhMT. Recombinant human $\beta\alpha$ -rhMT has the sequence shown in Figure 1 with 20 cysteine residues binding 6 As^{3+} leaving 2 uncoordinated cysteine residues¹⁰⁶. The α -rhMT and β -rhMT fragments each bind 3 As^{3+} . The full rfMT protein has 16 cysteine residues divided into two domains: a 9 residue C-terminal domain, β -rfMT, capable of binding 3 As^{3+} and a 7 residue N-terminal domain, γ -rfMT, capable of binding 2 As^{3+} for a total of 5 As^{3+} . The figure shows that while the rate constant for the 3 metal fragment, β -rfMT, matches the β -rhMT, the 2 As^{3+} fragment, γ -rfMT, is unique. Reprinted with permission from ref⁷⁴ copyright (2009) American Chemical Society.

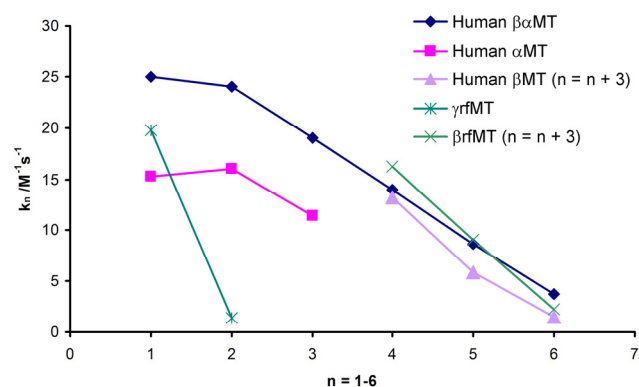


Figure 6. Comparison of the rate constants calculated from time-resolved ESI-MS measurements for As^{3+} metallation of α -rhMT, β -rhMT, $\beta\alpha$ -rhMT, γ -rfMT, and β -rfMT. The rate constant data for β -rhMT and β -rfMT were drawn with the value of n shifted by 3 to illustrate the similarity to the rate constant trend of the final three As^{3+} binding to $\beta\alpha$ -rhMT. Recombinant human $\beta\alpha$ -rhMT has the sequence shown in Figure 1 with 20 cysteine residues binding 6 As^{3+} leaving 2 uncoordinated cysteine residues¹⁰⁶. The α -rhMT and β -rhMT fragments each bind 3 As^{3+} . The full rfMT protein has 16 cysteine residues divided into two domains: a 9 residue C-terminal domain, β -rfMT, capable of binding 3 As^{3+} and a 7 residue N-terminal domain, γ -rfMT, capable of binding 2 As^{3+} for a total of 5 As^{3+} . The figure shows that while the rate constant for the 3 metal fragment, β -rfMT, matches the β -rhMT, the 2 As^{3+} fragment, γ -rfMT, is unique. Reprinted with permission from ref⁷⁴ copyright (2009) American Chemical Society.

Figure 6 provides rate constant data for As^{3+} binding to the MT protein from *Fucus vesiculosus* (rfMT) and compares it to the As^{3+} data obtained for recombinant human MT-1 (rhMT). These data illustrate the effect of linker size on the association constants of the protein. In the case of rfMT, the 14 amino acid interdomain linker altered the kinetics such that each domain binds As^{3+} in an effectively isolated fashion; that is, the two domains are sufficiently separated so as to not communicate with each other. Whereas, in the case of rhMT-1, the two domains are separated by a distance of 6 amino acids and it is this closeness that allows for the summation of the association constants. Plant and wheat MTs provide further species with which to test the linker dependence of the dependence of the metallation rate on available sites as there are a range of linker lengths found.

In addition to changes in the kinetics of metal binding, a critical study by the Huang group has shown that by systematically increasing the length of the MT linker found in Chinese hamster ovarian cells (MT-2), metal-ion tolerance may be impacted⁹⁹. Importantly, as the length of the interdomain linker region increases, the organism's tolerance for metal-ions decreases. Further, as linker length increases, the number of detectable MT molecules decreases suggesting that the added flexibility of the linker renders these forms are more susceptible to proteolysis. When placed in the context of the kinetic data, these mutational studies suggest that the linker region is critical in modulating the metal-ion affinity of MT, as well as its *in vivo*

stability. When the linker is extremely short, such as the 3 amino acids found in naturally occurring human MT-2a, the high affinity favours metal-ion sequestration and detoxification, such as Hg^{2+} or As^{3+} . When the linker increases in size, the ability to detoxify metal ions decreases, and this may favour its homeostatic function (Zn^{2+} or Cu^+). Recalling that as the linker length increases so the advantage of a large number of equivalent and accessible metal binding sites decreases and the magnitude of the binding constant diminishes. In this last case, the increased linker size also creates the potential for an as yet unknown secondary structure to exist within the linker itself. This secondary structure could then allow MT the ability to preferentially interact with certain apo-enzymes and further support metal-ion homeostasis in the organism.

In addition to As^{3+} , extensive spectroscopic kinetic analyses of metallation has been performed on Cu^+ , which binds to three cysteine residues within milliseconds, but whose structural rearrangement to establish equilibrium requires upwards of 20 minutes¹⁰⁰⁻¹⁰¹. Because of the initially fast binding of Cu^+ to MT, a mass spectral kinetic analysis cannot be carried out on the system, however, the spectroscopic results provide some evidence that once bound, the individual metal-ions are fluxional and will migrate to the lowest energy site. From these results, it is tempting to postulate that the each metal ion may bind to a number of metal-binding sites, but that once bound they continue to be sufficiently mobile to allow for a preferred site to be occupied. In this manner, MT may be metallated in a site-specific manner.

The examples described above introduced the rather straightforward mechanism of As^{3+} binding, straightforward because the presence of the nonbonding pair of electrons on the As^{3+} appears to stabilize a trigonal pyramidal structure, which by stoichiometric analysis always adopts the bead-like model to accommodate the As^{3+} .¹⁰⁶ The question about when cluster formation begins for Zn^{2+} , Cd^{2+} , and Cu^+ , to identify the best studied of the metals that binding to MT, is related to the point at which cysteinyl thiolate bridging takes over from the terminal thiolate coordination of the As^{3+} binding sites.

With the comprehensive understanding of the mechanism of metallation, the remainder of this review focuses on understanding the different stages of metallation – from the initial metal-free protein to the partially metallated protein, and on to the supermetallated MT. In each case now, we identify the differences between the conventional view of a two-domain protein for, as examples mammalian MTs, and the case for a single domain protein, albeit with many binding sites as noted for the As_nMTs .

4. Single Domains: Apo-metallothionein

One area of particular importance to our understanding of the initial posttranslational metallation of MT, but for which little structural information exists, is the structure of the apo- or metal-free protein. One recently characterized example of a single domain metallothionein is that of the yeast copper metallothionein by Calderone *et al.*²⁹. In this paper, the authors demonstrate that yeast MT exists as a single domain, oligonuclear

Cu^+ -thiolate cluster, the largest known to biology. Importantly, the authors are able to posit that in addition to acting as a storage medium for copper, the thiolate cluster also allows for metal-exchange to occur.

It is the solution structure of the metal-free or apo-MT that impacts both the rate and mechanism of the subsequent metallation and is, therefore, central to MT's functional properties in the cell, with the possible accessibility of the 20 cysteine thiols to oxidation. An important study by Vallee and coworkers, in which a fluorescence labelling method for apo-MT was developed, demonstrated the presence of a significant pool of apo-MT (between 9% in the testis and 54% in the kidney) in the presence of metallated MT¹⁰². This paper relied on fluorescence spectroscopy, a technique that provides a weighted average of metallation, and assumes that MT is completely metallated (Zn_7MT), consequently the % amount of apo-MT, while present, may be an estimate of the maximal amount of apo-MT. Importantly, however, this paper suggests that apo-MT exists as a stable species and one may therefore infer that it is able to take part in cellular chemistry, specifically in the oxidative balance of the organism. Because the structure of a protein must dictate its function (the structure-function relationship), it is now clear that the structure of apo-MT must be significant in any possible cellular chemistry. In the experiment above, the presence of stable partially metallated protein is also possible as described for $\text{Zn}_5\text{-MT-1}$ above.

While there are an infinite number of possibilities for the solution structure of the apo-MT we can suggest two generalized possibilities: (i) apo-MT exists as a loose, denatured random-coil, where the cysteines would be directly exposed to the solvent and prone to oxidation, and (ii) alternatively, that apo-MT adopts a tighter conformation, where the cysteines would be more protected and resistant to oxidation.

NMR spectroscopic studies have suggested that the metal free protein lacks any traditional secondary structure and exists as a random-coil⁷ unlike the fully metallated MT, for which the addition of 28 cysteinyl-metal bonds adds significant structure. This result is further supported by CD spectroscopic data, where little secondary structure was observed for apo-MT²⁵. However, these results depend on the specific structural information provided by the technique. As we discuss in detail below, computational results and very recent mass spectral data for mammalian MT-1 indicates that both the apo-MT-1 and fully metallated MT-1 have similar charge state envelopes indicating that while they may be structurally dissimilar, the overall volume occupied by each species is roughly the same at neutral pH.⁶⁶ It should be noted that the pH may alter the overall size of the protein. For the remainder of this section, we will discuss first the computational models of apo-MT-1, as well as how these models contribute to our understanding of current experimental work and then the more recent experimental data that support a globular structure for apo-MT-1 at neutral pH.

4.1 Computational modelling of apometallothionein

Probing the structure of a peptide chain that is highly fluxional and does not include chromophorically useful residues is

problematic, and much of the available information on the possible structures of the apo-MT is the result of molecular modelling calculations by Rigby *et al.*⁶³⁻⁶⁵. These studies reported detailed molecular models of the apoprotein and are based upon a modified molecular mechanics/molecular dynamics (MM3/MD) force field¹⁰³. In these computational studies, the cysteinyl-thiolates were found to lie on the exterior of the peptide regardless of the initial conformation of the protein. Further, the number of hydrogen bonds in the protein increased upon removal of each metal ion. Consequently, when every metal ion was removed a significant network of hydrogen bonds existed, which was shown to help stabilize the structure of the now metal free protein.

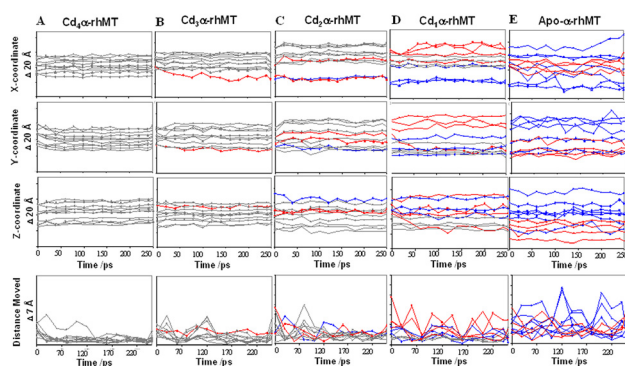


Figure 7. The motion of the 11 cysteinyl sulphurs in the α -domain in the x, y, and z directions over a 250-ps molecular dynamics calculation (top 3 plots). Plot of distance moved in Å for each of the 11 cysteinyl sulphurs in 3D space from the previous position in the MD calculation for the duration of the 250 ps (bottom plot). **A:** Cd₁- α -rhMT. **B:** Cd₃- α -rhMT. **C:** Cd₂- α -rhMT. **D:** Cd₄- α -rhMT. **E:** apo- α -rhMT. (—■— Cys-1; —×— Cys-2; —●— Cys-3; —▲— Cys-4; —◆— Cys-5; —■— Cys-6; —*— Cys-7; —+— Cys-8; ——— Cys-9; ——— Cys-10; —◆— Cys-11). The lines are colored coded as follows: Gray - cysteine thiolates coordinated to metal; blue - freed cysteine thiols from preceding removal of Cd; red - the motion of the cysteine thiols that were released by removing the current metal as indicated at the top of each column. Reproduced from Rigby *et al.*⁶⁴ with permission from John Wiley & Sons, Inc. (2006).

It is important to note, that even with the addition of a significant number of hydrogen bonds, the protein is still more fluxional than its fully metallated counterpart. This is demonstrated in Figure 7, which shows the motion of all eleven cysteinyl sulphurs in the α -domain of recombinant human MT. Upon successive demetallation of the domain, the backbone becomes progressively more flexible as a result of the cysteinyl thiols occupying their new position on the exterior surface of the protein. Importantly, this form has structure but could still be considered a random coil due to its inherent fluxionality, and a lack of a traditional secondary structure.

4.2 Apometallothionein may be folded as tightly as Zn₇-MT-1 at neutral pH

More recent structural information about apo-MT-1 has been provided by ESI mass spectrometry. This technique discriminates between different species based upon both their mass-to-charge ratio. Both the mass and the charge of a species provide unique information. In the first case, the mass of the species provides information on the homogeneity of a sample, both the number and the type of metal-ion can be determined as well as the presence of differently metallated MT species. In the second case, the charge state manifold of the species provides the experimenter with information regarding the overall fold of the protein. Large unfolded proteins occupy a significantly larger volume than folded proteins and are, therefore, able to stabilize a number of different charge states, while small well-folded proteins occupy a much smaller volume and are, therefore, only able to stabilize a small number of charge states.

While ESI-mass spectral data cannot provide the structural resolution afforded by X-ray crystallographic or NMR studies, this technique does provide a way of comparing the overall volume occupied by different MT species — their overall fold — while simultaneously allowing confirmation of the homogeneity of the sample¹⁰⁴. Perhaps most importantly, ESI mass spectral experiments may be performed on very dilute solutions (~10 μ M) at physiologic pH values, unlike X-ray crystallographic studies for which MT is notoriously difficult to crystallize for or NMR studies requiring millimolar (mM) concentrations of protein. In these regards, ESI-MS is capable of being performed on protein solutions much more similar to those one may expect in an organism.

A recent report from the Stillman group, examined changes in the overall conformation of the recombinant human apo-MT-1 upon exposure to the cysteine-modifying benzoquinone (Bq)⁶⁶. In that study, experimental structural data for the apo-protein was based on changes in the charge state distribution of the ESI mass spectral data⁶⁶. Importantly, the study aimed at examining the effects of modifying each of the twenty cysteine residues with the more hydrophobic aromatic ring of benzoquinone. Specifically, this experiment allowed for the determination of the cysteine residues, either located on the exterior of the protein, as Rigby *et al.* had suggested, or located interiorly, as might be expected if one were to simply remove the metal ions from the fully metallated protein. Interestingly, as Figure 8 shows there is little change in the charge state distribution between apo-MT-1 and the fully bound Bq₁₁-MT-1, strongly supporting the view that each cysteine residue is located on or close to the exterior surface of the protein, and further that covalent bonding of these cysteinyl thiols with Bq does not appreciably alter the overall fold of the protein. The authors note a slight increase in the charge state envelope with the maximum intensity charge state transitioning from 5+ to 6+ at 11 Bq:MT, and this is expected due to an increase in the molar mass, and therefore overall volume, of the protein⁹¹. This result is further supported by calculated changes in volume using the NIH calculator¹⁰⁵. These results now provide experimental evidence supporting the existence of cysteines on the exterior surface of the apo-MT protein.

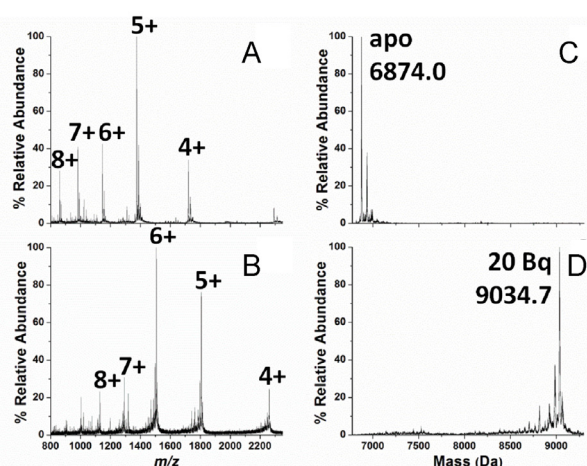


Figure 8. ESI-mass spectra measured at pH 5.5 showing the complete coupling of Bq to the cysteinyl sulphurs in the full apo- β -rhMT-1. (A, B) show the charge state distribution with the corresponding deconvoluted spectra (C, D). Importantly a single Bq molecule coordinates to each cysteine residues leading to a total of twenty cysteine residues binding to form the final Bq₂₀-MT-1 product. Reproduced from ref⁶⁶ with permission from Elsevier (2012).

This same study also highlights an additional structural consideration, which is that both apo-MT-1 and fully metallated Zn₇-MT-1 share an almost identical charge state profile indicating that they in fact occupy a similar overall volume as shown in the early computational studies of Rigby, et al. Figure 9 shows the charge state mass spectra for the three significant species in metallothionein chemistry: the metal-free apo-protein at pH 7, the fully metallated holo-protein at pH 7, and the apo-protein at pH 3. Unlike the previous experimental setup, where a single Bq molecule terminally bound to a single cysteinyl sulfur, the presence of metal-thiolate bonds necessitates the internalization of the cysteine residues¹⁰⁶. However, molecular modeling of the M₇-MT-1 suggests that unlike the solid-state X-ray structure (of rat liver Cd₅Zn₂-MT)²¹, which exhibits a well-formed two-domain shape, the domains essentially appose in solution (Figure 10) and the resulting solution structure is, therefore, somewhat similar to the apo-MT structure⁶³.

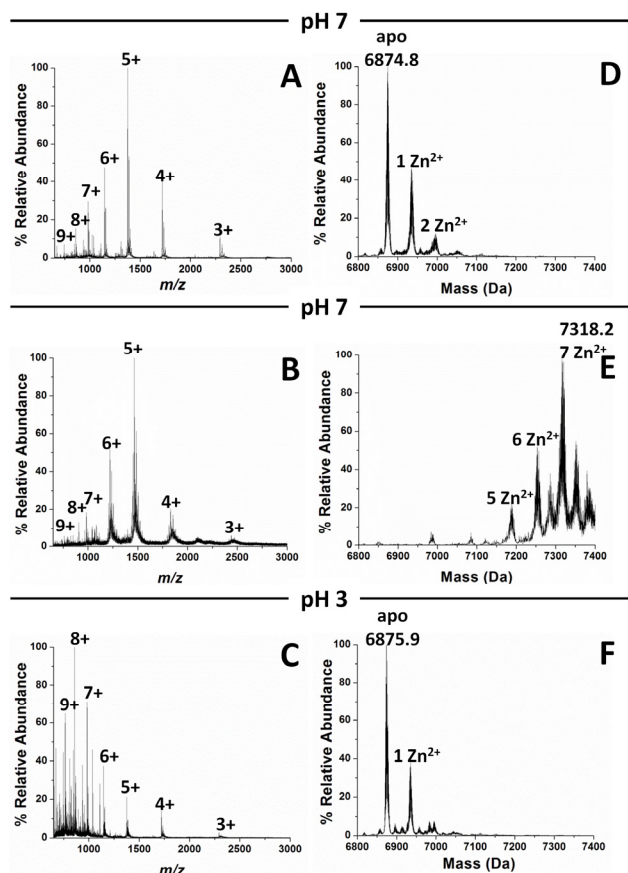


Figure 9. ESI-mass spectra recorded for rhMT-1. The charge state spectra for apo-rhMT-1 at pH 7 (A), fully metallated Zn₇-rhMT-1 at pH 7 (B), and demetallated apo-rhMT-1 at pH 3 (C). (D) The deconvoluted spectrum from (A), showing the mass of apo-MT-1 as 6874.8 Da. A slight Zn²⁺ impurity can be seen in this spectra. (E) The deconvoluted spectrum from (B) showing the mass of Zn₇-rhMT as 7318.2 Da. (F) The deconvoluted spectrum from (C) showing the mass of apo-rhMT is 6875.9 Da following acid-induced demetallation. Importantly, the charge state envelopes (A, B, C) provide strong evidence that the overall volume of Zn₇-rhMT and apo-rhMT at pH 7 are roughly equivalent, but that under extremely acidic conditions (pH 3) the protein occupies a significantly larger volume. Reproduced from ref⁶⁶ with permission from Elsevier (2012).

45

In fact, the only significant change to the charge state manifold is observed when the pH of the solution is lowered from 7 to 3 (Figure 9). The low pH charge state spectrum is quite different compared with the data measured at pH 7. The dominant charge state at pH 7 is 5+, while that at pH 3 it is 8+. This shift to higher charge states indicates that at lower pH values, the MT opens up and occupies a larger effective volume. This is an expected result given that at lower pH values, both more acidic and basic residues will be protonated altering the overall charge of the protein.

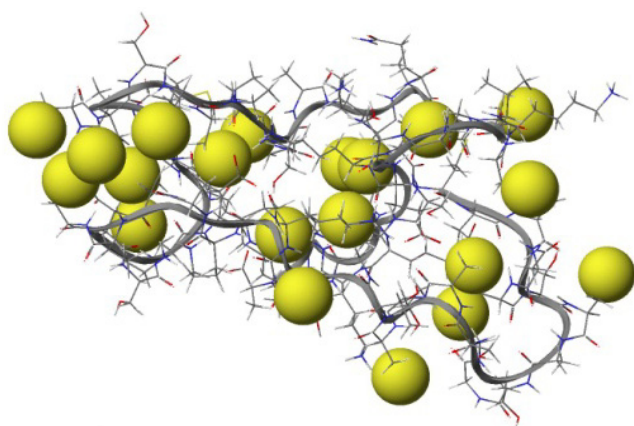


Figure 10. Molecular model of the 20 cysteines in apo- β MT-1. In the absence of metal-ion coordination, the cysteinyl sulphurs (shown as yellow space-filling spheres) move to locations on the exterior surface of the protein. This structure was minimized in two steps: 1) 1000 ps at 500 K, and 2) 5000 ps at 300K. The conformer with the lowest energy is presented above. The initial structure of the Cd- β -rhMT-1 was provided by Chan et al.¹⁰⁴. Reprinted with permission from ref³⁵ copyright (2013) American Chemical Society.

5. Single Domains: the case for Zn₅-MT-1

The metallation properties of MT with Zn²⁺ are significant because zinc is an essential element with a large number of distinct roles in a number of cellular processes¹⁰⁷⁻¹⁰⁹. For example, fully metallated Zn₇-MT has been considered an intricate component of the cellular redox cycle because this species is able to simultaneously deactivate oxidative molecules through the oxidation of its own thiol groups to disulfide bonds, and is able to release Zn²⁺ ions⁵⁴ into the cellular environment where they are able to upregulate DNA transcription through the zinc finger transcription factors of a number of proteins, including MT itself¹⁰⁻¹¹¹. Recent implications of the release of Zn²⁺ from intracellular stores to phosphorylate kinases that are involved in both cell proliferation and migration underscore this element's importance in the cell signaling cascade – a cascade which may be of pharmacologic importance in designing new anticancer drugs¹¹².

Further, the reports that MT binds metals in a noncooperative fashion, that is each metal ion binds ‘one at a time,’ suggests the possibility that partially-metallated species are stable and are able to take part in cellular chemistry^{36, 39-40, 73}. The isolation and characterization of these partially-metallated intermediates is currently an area of significant interest.

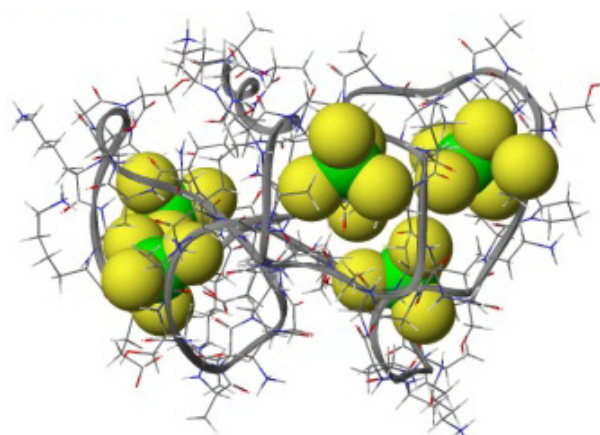


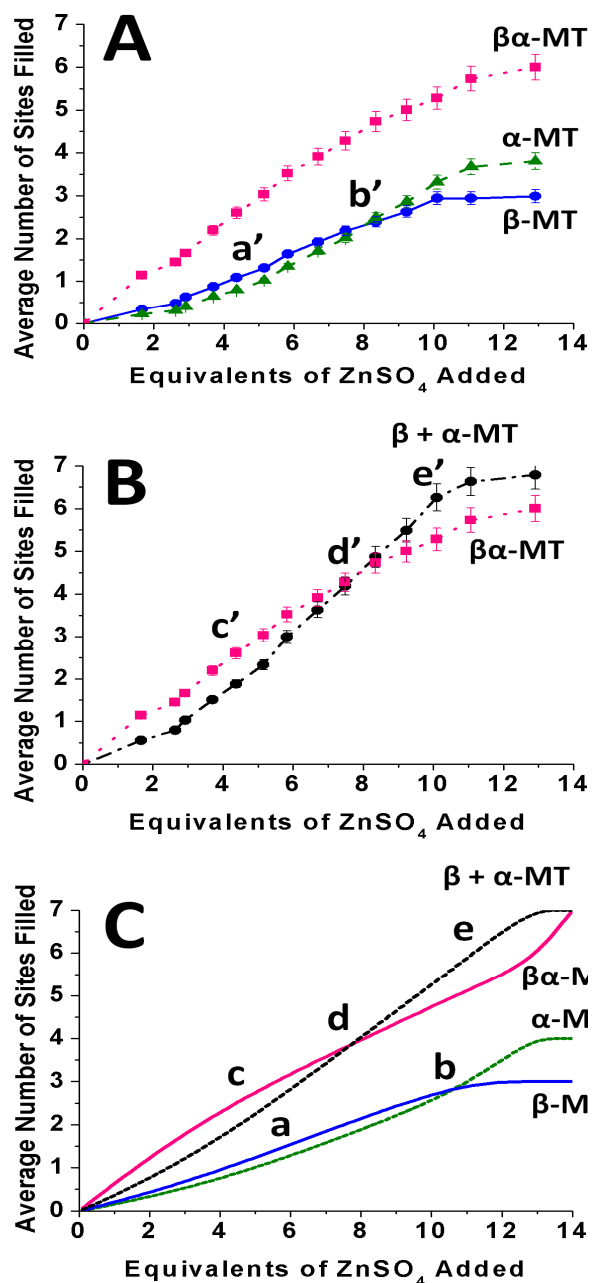
Figure 11. Molecular model of Zn₅-rhMT-1. The single domain Zn₅-rhMT-1 structure was created by assigning a single Zn²⁺ ion to every 4 consecutive cysteine residues. This structure was minimized in two steps: 1) 1000 ps at 500 K, and 2) 5000 ps at 300K. The conformer with the lowest energy is presented above. The initial structure of the Cd- β -rhMT-1 was provided by Chan et al.¹⁰⁴. Reprinted with permission from ref³⁵ copyright (2013) American Chemical Society.

One intermediate that is gaining in importance in the metallation mechanism of MT with Zn²⁺ is that of Zn₅-MT³⁵. The existence of this species was determined through the direct competition of the isolated α - and β -domains of recombinant human MT-1 with the full β -protein for a limiting quantity of Zn²⁺.³⁵⁻³⁶ A molecular model of the potential structure of Zn₅-MT-1 is presented in Figure 11. The important aspect is that each zinc ion is coordinated to exactly four cysteine residues in the terminal fashion described above for As³⁺..

The experiment used to elucidate the existence of the beaded Zn₅-MT-1 exploited the resolving power of ESI-mass spectrometry and was designed to determine the existence of any domain-domain interactions within metallothionein. By using the mass spectrometer to track all species simultaneously, we designed a competition experiment that was able to determine the exact speciation in solution. This experiment allowed, for the first time, the determination of association constants for each metal with the full MT simultaneously with the two isolated domains. The design involved two zinc competition experiments: (i) a two-way competition in which the two isolated fragments containing the α - and β -domains competed for the zinc added in a stepwise manner, and (ii) a three-way competition that introduced the full, apo- β -MT to the solution of the two fragments. The key experiment was the three-way competition experimental design where there were initially 14 binding sites available to the incoming zinc. The details of the design and the full results were first described in the Ph. D. Thesis of Sutherland¹¹³.

The rationale behind this experiment was that if the two well-known domains of the full protein (β and α) behaved as isolated units as considered previously, then the observed binding constants of the full MT protein would equal the sum of the two isolated domains in the isolated fragments. The 14 binding sites would align as two sets of 7 binding sites (7 and 4+3). On the other hand, if the complete protein acted as a single peptide of 20 cysteines as a single domain of potentially 5 binding sites but the

two isolated fragment peptides act as two single domains containing 11 (α domain fragment) and 9 (β domain fragment) cysteines there would be differences in the metallation distribution determined by the ESI-mass spectral experiment at equilibrium. In this case, the As^{3+} metallation data³¹⁻³⁴ suggest K_1 for the three strands to be quite different, with K_1 (full protein) to be significantly larger than either of the K_1 's for the two isolated domains.



10 **Figure 12. Experimental and simulated metallation states of apo- β -rhMT-1, apo- α -rhMT-1, and apo- $\beta\alpha$ -rhMT-1 when metallated with Zn^{2+} under competitive conditions. (A)** Average number of Zn^{2+} ions bound in the β -domain (blue), the α -domain (green), and the full MT protein (red). (B) Comparison
 15 of the average metallated states of the sum of the two domains (black -•-) and the full protein as a function of added Zn^{2+} . (C)

Simulation of the stepwise distribution of Zn^{2+} among the three protein species using the $\log_{10}(K_F)$ values of 12.6, 12.3, 11.8, and 11.5 for the α -domain, 12.7, 12.4, and 12.0 for the β -domain, and 20 13.3, 13.1, 12.7, 12.4, 12.0, 11.3 and 10.8 for the full MT protein. The key features (a'-e') in the experimental data (A) and (B) are modelled in the simulation shown in (C) as a-e, respectively). Reprinted with permission from ref³⁵ copyright (2013) American Chemical Society.

In the early stages of this metallation experiment the full protein outcompeted the isolated domains for the available Zn^{2+} up to 6.4 equivalents, however, surprisingly past this point the 30 isolated domains were able to actually outcompete the full protein for the remaining Zn^{2+} ions (Figure 12 A and B). To understand the control exerted by the series of 14 K's, the data were modeled with a series of 14 independent bimolecular equations (Figure 12C).

35 Guidance for the modeling of the association constants (Figure 12C) was based upon the previously published work by Ngu *et al.*, which showed that the affinity of MT for As^{3+} was directly related to the number of available metal binding sites^{31-34, 74}. Using the As^{3+} metallation results as a model, we would expect 40 the association constant to decrease statistically as each As^{3+} binds and occupies one of the available metal binding sites. Previous reports for zinc binding by Krezel and Maret⁷⁰, clearly demonstrated the existence of a decreasing series of association constants for MT, and their work was useful in demonstrating 45 that the metallation of MT is, in fact, noncooperative. However their work did not extract the exact association constants for both the full MT protein, and those for the isolated domains. It was the three-way competition experimental that provided the key information. From the mass spectral data recorded during the 50 zinc titrations, the location of the incoming metal (full protein or one of the isolated domains) could be explicitly determined. Further, since the binding constants for the three slightly different ligands were so similar there was equilibrium between all species and the ratios of the three sets of K's acted to distribute the zincs 55 between the three peptides in a quantitative manner. In this way, the slight differences in the K's were signaled by the differences in the metallation ratios over a larger range of zinc concentration.

The association constants for the modeled data that provided the best match to the experimental data were as follows: α -domain 12.6, 12.3, 11.8, 11.5, β -domain 12.7, 12.4, 12.0, full $\beta\alpha$ -protein 13.3, 13.1, 12.7, 12.4, 12.0, 11.3, and 10.8. Significantly, the decrease in the binding affinity of MT for Zn^{2+} occurs in a fairly linear fashion until the formation of Zn_5 -MT at which point there is a substantial decrease in the association constants. This 65 decrease is attributed to the requirement for bridging metal-thiolate clusters to form. Surprisingly, a significant drop in affinity is not observed in the isolated domains leading to the formation of Zn_4 - α -MT and Zn_3 - β -MT and this strongly implies that specific domain-domain interactions or rearrangements are 70 necessary for the formation of clustered Zn_6 - $\beta\alpha$ -MT and Zn_7 - $\beta\alpha$ -MT.

The proposed model requires that metallation is noncooperative and metallation up to 5 Zn^{2+} is not domain-specific because no clustered domains exist at this point. It is

probable that the 6th Zn^{2+} that adds to form Zn_6 -MT adds in a domain-specific manner forming either the α - or β -domain, but while it is clear that domain-domain interactions must occur, it is unclear which domain is formed first. Previous NMR spectroscopic work by Good *et al.* clearly demonstrate the formation of the α -domain prior to the β -domain, however, the NMR signals associated with the β -domain are significantly weaker than those of the α -domain, and it is possible that their signals were masked^{30, 44, 97}. Consequently, further competition experiments involving NMR spectroscopy will likely be necessary to elucidate the location of the final metal-binding sites.

6. Single Domains: Supermetallation of MT

The conventional view of Zn_7 -MT is that metallation with Cd^{2+} will lead to the formation of Cd_7 -MT, both having an almost identical 3-D molecular topology^{21, 68-69, 114}. However, it is still unclear exactly how this fully metallated protein is capable of exchanging metal-ions. For example, recently work in the field of Alzheimer's disease (AD) by Vasak and coworkers¹¹⁵⁻¹¹⁸ demonstrated that Zn_7 -MT-3, a brain specific metallothionein, is capable of exchanging metal ions with $A\beta_{1-40}$ - Cu^{2+} forming Cu_4Zn_4 -MT-3 and $A\beta_{1-40}$ - Zn^{2+} . By exchanging the redox inactive zinc for the redox active copper, MT inhibits a significant amount of oxidative stress that is a hallmark of AD. Importantly, MT-3 was first discovered as an abundant protein in normal human brains, but was lacking in the brains of those with AD⁵².

The recent discovery of a number of supermetallated forms of the MT protein may help to elucidate the mechanism of metal exchange in MT. Supermetallation may be defined as metallation in excess of traditional levels^{3, 30, 39, 44}. Further NMR studies suggest that the traditional two-domain structure is capable of collapsing into a single-domain. Specifically, it has been shown for MT-1 and -3 that Cd_7 -MT (a two-domain structure) is capable of coordinating an additional Cd^{2+} ion to form Cd_8 -MT (a one-domain structure)^{30, 44, 117, 119}. While both the α - and β -domains of human MT-1 have each been shown capable of binding exactly one extra Cd^{2+} forming Cd_5 - α -MT-1 and Cd_4 - β -MT-1^{44, 119}. This has significant consequences for two critically important questions in MT research: 1) how does metallated MT equilibrate metal ions with the surrounding cellular environment? and 2) how do the β - and α -domains of MT exhibit metal ion selectivity?

The first question is important for the cellular function of MT as both a cellular buffer of the essential metals, such as zinc and copper, as well as a cellular sink for the toxic ones, such as cadmium and arsenic. Metal transfer reactions in MT have been well documented, for example the Zn^{2+} transfer of fully metallated Zn_7 - β -MT to m-aconitase⁹³, carbonic anhydrase¹²⁰⁻¹²¹, and the prototypical transcription factor Gal4¹²². *In vitro* metal-exchange experiments have shown that both Cd^{2+} and Hg^{2+} are readily able to replace Zn^{2+} from Zn -MT-2^{23, 123}. Further, removal of Zn^{2+} from the zinc finger-containing transcription factor Sp1 demonstrates that MT may also act as a Zn^{2+} acceptor¹²⁴. While these studies demonstrate the metal-ion

exchange does occur, in none has an intermediate been characterized that would provide insight into the actual mechanism of metal transfer.

The second question is also of critical importance to the function(s) of MT. Importantly, NMR studies of MT have shown that the conventional fully metallated clusters (that is Zn_3Cys_9 and Zn_4Cys_{11}) are effectively isolated from each other^{68-69, 114, 125}. Further, the metal ion selectivity of these clusters leads to an accumulation of Zn^{2+} ions in the α -domain, and Cu^+ ions in the β -domain. Taken together, these results suggest that each domain of MT is responsible for different functions *in vivo*. However, given the available NMR data, it is unknown exactly how the fully metallated and effectively isolated domains interact with one another to allow for metal-ion exchange unless the model described above for Zn_5 -MT-1 and illustrated below also is involved.

In support this view we can consider a recent report by Manso *et al.* who have demonstrated that the full MT-1 was able to improve the performance of MT knockout mice whose cortex had been damaged through cryoinjury^{57, 126}. Most interestingly, the authors report that exposure of the mice to the isolated β - and α -MT fragments result in markedly different recovery rates compared to the full $\beta\alpha$ -protein. While the exact mechanism of action is not known, it is plausible that critical domain-domain interactions found in the supermetallated state of the protein may be a causative agent in their recovery.

In the case of zinc homeostasis, the protein appears to be important to the viability of an organism when exposed to the extremes of zinc availability. MT-1 and MT-2 knockout mice were shown to be delayed in their renal development when, as pups, they were fed severely deficient diets, while adult knockout mice challenged with increased Zn^{2+} had a greater incidence of pancreatic acinar cell degeneration¹²⁷.

In the case of copper homeostasis, the protein also appears to be important to the viability of organisms with respect to copper toxicity. Unlike zinc, free copper is able to catalyze the formation of hydroxyl radicals through Haber-Weiss and Fenton reactions¹²⁸. The two most well known copper related disorders include Menkes disease, and Wilson's disease¹²⁹. In both diseases, MT has been reported as beneficial in ameliorating symptoms. In the first case, a murine model of Menkes disease involving MT-1 and -2 knockout mice demonstrated that in the absence of inducible MT, knockout mice were more susceptible to copper toxicity¹³⁰. In the case of Wilson's disease, accumulation of Cu-MT somewhat mitigates cellular damage, because the 20 cysteinyl thiols are capable of both reducing Cu^{2+} to Cu^+ and sequestering these ions^{26, 131}.

These examples illustrate the importance of MT in metal ion homeostasis. The ability of each domain to act as an effectively 'isolated' compartment would allow for MT to take part in both Zn^{2+} and Cu^+ homeostasis simultaneously, while returning to the holding pattern of the single-domain, bead-like structure.

However, prior to the characterization of the supermetallated MT, there was no metal-exchange intermediate that would allow each domain within MT to reach equilibrium. Without this intermediate, the only reasonable explanation would be

equilibration via a series of association-dissociation events between MT and the surrounding media. In addition, these events would need to be domain specific, meaning that Cu^+ preferentially coordinated with the β -domain and $\text{Zn}^{2+}/\text{Cd}^{2+}$ preferentially coordinated with the α -domain^{22, 100}. Experimental evidence directly disputes this last requirement, as displacement of Zn^{2+} from $\text{Zn}_7\text{-MT}$ by Cu^+ occurs in a distributive manner (binding to both domains) followed by a time- and temperature-dependent rearrangement leading to the expected metal ion selectivity¹³²⁻¹³³.

It is possible that MT is able to achieve metal ion equilibrium through both the bead-model structure mechanism and through these supermetallated states. Briefly the coordination of an exogenous metal ion to $\text{Zn}_7\text{-MT}$, such as Cd^{2+} or Cu^+ , leads to the transient formation of a $(\text{Cd or Cu})_1\text{Zn}_7\text{-MT}$ followed by a rearrangement and subsequent expulsion of one of the previously bound Zn^{2+} ions to form $(\text{Cd or Cu})_1\text{Zn}_6\text{-MT}$ with the expected metal ion specificity. Below we will describe supermetallation of the isolated β -domain, $\text{Cd}_4\text{-}\beta\text{-MT-1}$, the isolated α -domain, $\text{Cd}_5\text{-}\alpha\text{-MT-1}$, as well as the full MT-1 protein, $\text{Cd}_8\text{-}\beta\alpha\text{-MT-1}$. The discovery of each of these intermediates was made possible by the use of cadmium, which has a significantly higher binding constant (10^3). This has allowed for these intermediates to be effectively 'frozen' by the higher binding affinity of cadmium ions for thiolate ligands.

Supermetallation of the α -domain of human MT-1 protein

The first reported instance of supermetallation was that of the α -domain, $\text{Cd}_5\text{-}\alpha\text{-rhMT}$. A characteristic feature $\alpha\text{-rhMT}$ is its biphasic, derivative-shaped signal, with positive extrema at 260 and 220 nm and a negative extrema at 240 nm^{1, 8, 25, 94, 134}. This derivative shape is attributed to the exciton coupling found in the four metal clusters. Upon addition of the 5th Cd^{2+} ion, a broad monophasic peak at 254 nm appears and demonstrates that this addition Cd^{2+} atom is directly interacting with the metal-thiolate cluster. However, only when advanced $^1\text{H}\text{-}^{113}\text{Cd}$ NMR techniques were used that allowed assignment of the possible connectivities of the supermetallated form of the cadmium-saturated α -domain was there conclusive evidence of the presence of this fifth metal ion bound to the cluster, Figure 13. This technique takes advantage of the ^3J scalar coupling constant between the cadmium ions and the β protons of the cysteine residues. In this way spectra may be acquired at a significantly faster rate (60 minutes vs. 60 hours) than a traditional 1- or 2-D ^{113}Cd experiment, and in addition the spectra also provide the connectivities of the Cd^{2+} ions, which can lead to a fast assignment of the overall structure of the cluster. The traditional NMR spectroscopic range Cd^{2+} coordination to thiols is between 600 and 700 ppm¹³⁵. From Figure 13, one can clearly see that of the five Cd^{2+} peaks four are located in this region, corresponding to the traditional CdS_4 units; however the fifth is significantly shielded and located at 224 ppm and is likely to represent $\text{Cd}(\text{RS})_2(\text{OH})_2$ ¹³⁶⁻¹³⁷. This octahedrally coordinated site is likely located near the cluster crevice, where a number of cysteinyl-sulphurs are exposed. Based on the chemical shift of the protons, this fifth Cd^{2+} ion is likely coordinated to cysteine residues 34 and 57 with significant structural rearrangement necessary to

accommodate the ion.

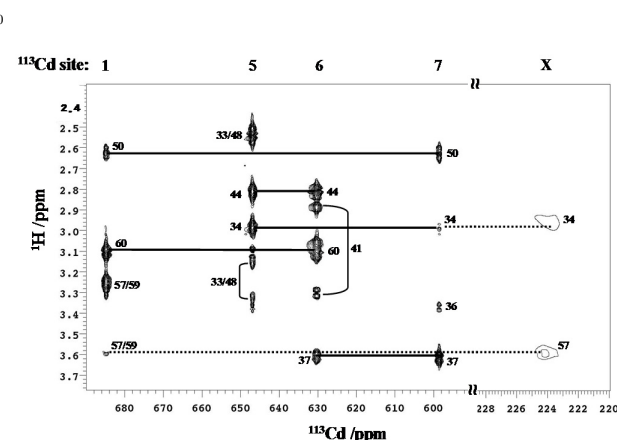


Figure 13. Determination of the cysteine-cadmium connectivities in the supermetallated recombinant human (rh) $\text{Cd}_5\text{-}\alpha\text{-rhMT-1}$. The Figure shows a combination of two indirect $2\text{D } ^1\text{H}\text{-}^{113}\text{Cd}$ HSQC NMR spectra for isotopically enriched $^{113}\text{Cd}_4\text{-}\alpha\text{-rhMT-1}$ titrated with an additional 10.0 molar equivalents of $^{113}\text{Cd}^{2+}$ to form the $^{113}\text{Cd}_5\text{-}\alpha\text{-rhMT-1}$ species. The spectra were recorded in the ^1H chemical shift range 2.3–3.7 p.p.m. and the ^{113}Cd ranges 590–690 p.p.m. ($^3\text{J} = 66$ Hz) and 220–245 p.p.m. ($^3\text{J} = 40$ Hz). This two dimensional plot shows how the HSQC technique can determine the connection between individual cysteine residues (y-axis) and individual cadmium atoms (x-axis). When two or more cadmium atoms share one cysteine residue, two signals with similar ^1H chemical shift range will appear for multiple cadmium atoms. The cadmium numbering scheme follows the original numbering scheme of Otvos and Armitage for the two-domain $\text{Cd}_7\text{-}\beta\alpha\text{-MT-2a}$ ¹⁴². Reproduced from ref¹¹⁹ with permission from John Wiley & Sons, Inc. (2008).

Supermetallation of the β -domain of human MT-1 protein

The β -domain of hMT-1 has also been an area of significant interest. Early studies involving CD spectroscopy¹³⁸ and ESI-mass spectrometry³⁹ provided evidence that suggested the supermetallation was indeed possible in the β -domain of hMT-1. This structure was of significant interest owing to the β -domains preferential involvement in copper homeostasis^{22, 101, 139}, as well as its involvement in MT-3 in brain chemistry, for which the β -domain differs by a TCPCP motif^{14, 140-141}.

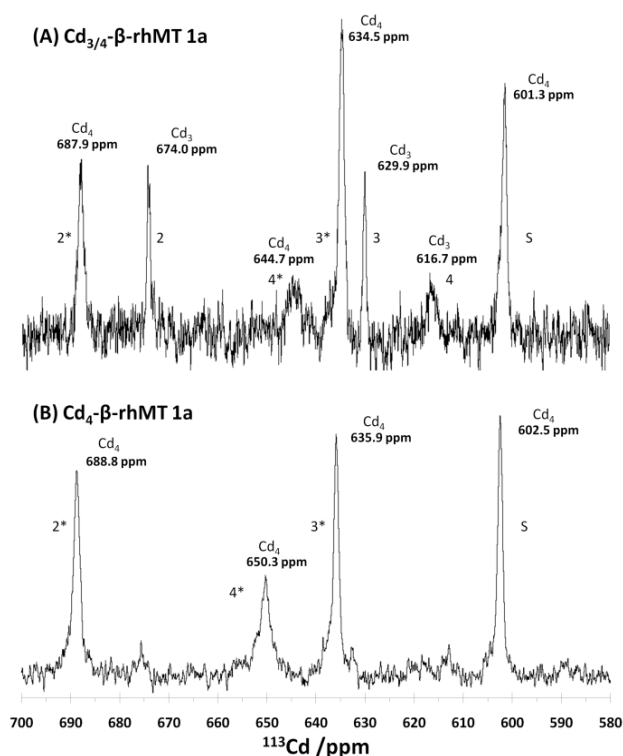


Figure 14. Direct 1D ^{113}Cd NMR spectra of (A) a mixture of Cd_3 - β -rhMT and Cd_4 - β rhMT-1 and (B) Cd_4 - β -rhMT-1 formed by the addition of excess $^{113}\text{CdCl}_2$. Slight shifts in the values of Cd_4 - β rhMT-1 were observed between the mixture and the pure supermetallated sample. This shift is attributed to the addition of chloride ions from $^{113}\text{CdCl}_2$ to the solution and is most pronounced in the least intense Cd_4 - β rhMT-1 signal at 644.7 ppm, with a total downfield shift of 5.6 ppm. Reprinted with permission from ref ⁴⁴ copyright (2010) American Chemical Society.

The NMR spectra of β -rhMT-1 are shown in Figure 14, where in (A) the spectrum is from a mixture of Cd_3 - and Cd_4 - β -rhMT-1, while (B) shows a spectrum of the pure Cd_4 - β -rhMT-1. The mixture in (A) is the result of a slight excess of $^{113}\text{CdCl}_2$ added to solution to stabilize the β -rhMT-1 against air oxidation. Briefly, in (A) the peaks associated with Cd_3 - β -rhMT are 674.0, 629.9 and 616.7 ppm, while those associated with Cd_4 - β -rhMT are 687.9, 644.7, 634.5, and 601.3 ppm. Importantly, none of the peaks are below 600 ppm, and no peaks were found in the ~ 200 ppm region. It should be noted, that the β -domain has been historically considered the less stable of the two-domains, this may be due to the inherently weaker ^{113}Cd signals found in the NMR, compared to the α -domain, which suggested enhanced fluxionality of the protein ^{7, 18-20, 97, 125}.

By adding an excess of $^{113}\text{CdCl}_2$, Figure 14B shows formation of only those peaks associated with Cd_4 - β -MT-1. In these two spectra, each peak falls between 600 and 700 ppm, a strong indicator that each cadmium centre is coordinated to a significant number cysteine residues. The supermetallated cadmium atom has been tentatively assigned to the peak corresponding to 602.5 ppm, which would suggest tetrahedral coordination to four thiolates, or three thiolates and a single water molecule/chloride

ion.

These data conclusively show that supermetallation of the β -domain is the result of a directly interaction of the 4th Cd^{2+} ion with the metal-thiolate cluster. This interaction results in significant rearrangement and further this coordination could potentially involve a water molecule/chloride ion. In both the isolated β - and α -domains, it is likely that the coordination sites that do not involve a thiol, for example where there is a water molecule or chloride, may be the result of the absence of the second domain. If both domains were present, then there would be sufficient thiol groups to allow for complete coordination of an incoming metal ion through both domains. This possibility has profound consequences on our understanding of MT as it relates to both metal-ion homeostasis and toxic metal-detoxification, since prior to the reports of these supermetallated structures it was considered that the only possible means for MT to reach metal-ion equilibrium between both its domains, and between itself and the surrounding environment would be through a series of association-dissociation events.

Supermetallation of the full human MT-1 protein

A series of reports have greatly contributed to our understanding of the supermetallation of the full human MT, including both MT-1^{30, 39} and the brain specific MT-3^{40, 117}. The view that a single metal ion is coordinated to both domains is supported from NMR spectroscopic studies of the two isolated domains of MT-1 (Figure 13 and 14) where the supermetallated metal ion is coordinated to several water molecules, which could be substituted for thiol groups from the adjacent domain.

(A) $\text{Cd}_{7/8}$ - $\beta\alpha$ -rhMT 1a

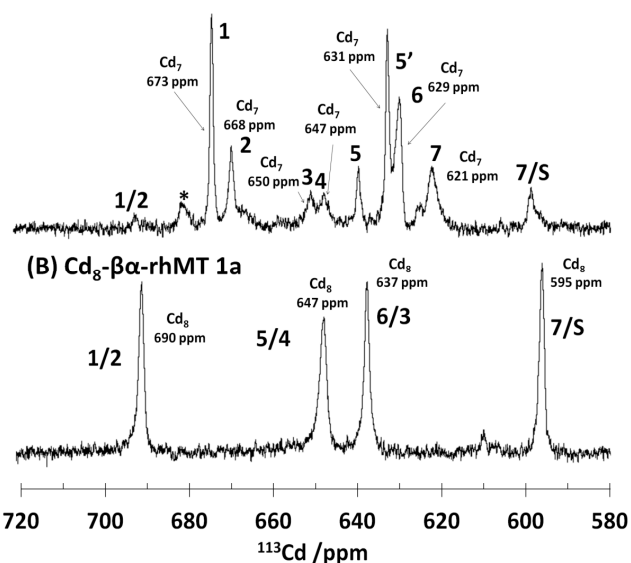


Figure 15. Direct 1D ^{113}Cd NMR spectra of (A) a mixture of Cd_7 - $\beta\alpha$ -rhMT and Cd_8 - $\beta\alpha$ -rhMT and (B) Cd_8 - $\beta\alpha$ -rhMT formed by addition of excess $^{113}\text{CdCl}_2$. An additional peak is present in $\text{Cd}_{7/8}$ - $\beta\alpha$ -rhMT at 680 ppm, labelled with an asterisk (*), which was observed in the original titration by Boulanger and Armitage¹⁹. Subsequent addition of solid $^{113}\text{CdCl}_2$ to $\text{Cd}_{7/8}$ - $\beta\alpha$ -rhMT led to the formation of Cd_8 - $\beta\alpha$ -rhMT, which greatly

simplifies the spectra reducing it to 4 peaks. Reprinted with permission from Sutherland *et al.*³⁰ copyright (2012) American Chemical Society.

The 1D ¹¹³Cd NMR spectroscopic data of both Cd₇- and Cd₈-β_α-rhMT-1 are shown in Figure 15. In the Cd_{7/8}-β_α-rhMT-1 spectrum (A), peaks 1, 5, 5', 6 and 7 correspond to the α-domain, while peaks 2, 3 and 4 correspond to the β-domain. Signals observed for Cd_{7/8}-β_α-rhMT include resonances at 673, 668, 650, 647, 631, 629 and 621 ppm, where the resonances at 673, 631, 629 and 621 ppm result from the α-domain and 668, 650 and 647 ppm result from the β-domain.

There are just 4 main signals for the pure Cd₈-β_α-rhMT-1 (B) at 690, 647, 637 and 595 ppm. The chemical shift range of all the peaks is between 590 and 700 ppm, which overlaps significantly with the region expected for tetrahedral cadmium-thiolate clusters. No signals in the range of 200 to 250 nm were observed, which had been previously observed for supermetallated Cd₅-α-rhMT. It is likely that Cd(RS)₂(OH₂)₄ unit found in the α-domain of MT was the result of the lack of the β-domain, and the requirement for thiols from this domain to complete the coordination sphere.

The addition of excess ¹¹³Cd²⁺ eliminates the spectral complexity of Cd₇-β_α-rhMT. The formation of only four unique peaks, from an initial seven, suggests that the two domains have effectively coalesced into one. It should be noted at this point, that while the NMR spectra for supermetallated MT-3¹¹⁷ are similar to those MT-1, they are not identical and it may be that these two isoforms achieve supermetallation through different structural rearrangements.

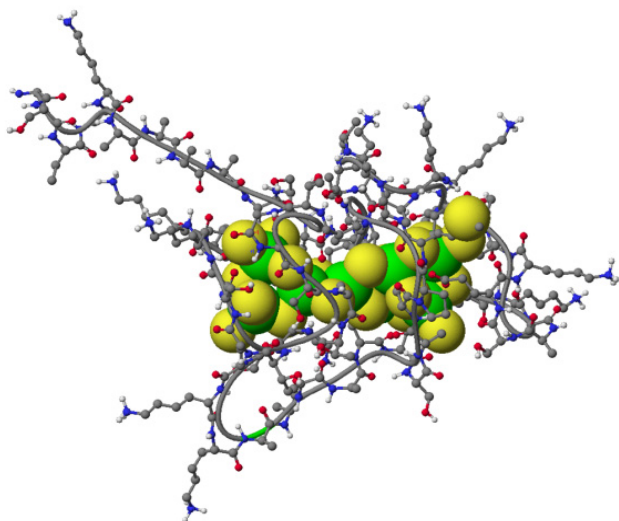


Figure 16. Molecular model of Cd₈-rhMT. This structure was minimized in two steps: 1) 1000 ps at 500 K, and 2) 5000 ps at 300K. The conformer with the lowest energy is presented above. The initial structure of the Cd₇-β_α-rhMT-1 was provided by Chan *et al.*¹⁰⁴. Reprinted with permission from Sutherland *et al.*³⁰ copyright (2012) American Chemical Society.

A model of a potential structure of Cd₈-β_α-rhMT-1 is provided in Figure 16. This model is for illustrative purposes and does not

necessarily reflect the true structure of supermetallated MT-1, which will require a complete NMR backbone assignment to determine. Importantly, the model demonstrates rather clearly that the linker between the two domains is not sufficient to hinder their interactions with each other. In fact, if one were to examine the sequence of MT, one would naturally assume a single 'super-cluster' since this division between adjacent cysteine residues is of similar length to others in the sequence. Future work will require an examination of the effects of linker length on the ability of MT to supermetallate.

One important question, which must be addressed in future research, is whether or not supermetallation is, in fact, a general characteristic of all MT proteins, or if it is specific to certain isoforms. Currently evidence exists for both human isoforms MT-1 and MT-3, however there does not exist any evidence to support or dismiss supermetallation in MT-2. It would be very surprising if MT-2 did not supermetallate, since both MT-1 and MT-2 are more closely related than MT-3, the formers having diverged before distinction of the mammalian orders and the latter, more structurally distinct, having evolved much earlier¹¹. However, given differences in the NMR pattern between supermetallated MT-1 and MT-3, it could be that slight structural differences between MT isoforms is what contributes to their distinct *in vivo* functions.

7. Conclusions

The results presented in this paper, support a paradigm altering view of MT, in which the two-domain nature of metallothionein is proposed to be a specific and specialized case with a single domain structure dominating at both low and high stoichiometric ratios.

In the early stages of metallation, many metal ions bind to apo-hMT-1 in a noncooperative manner. In the proposed general model based on the new experimental data summarized¹¹³ in this review, clustering, a key feature of metal-saturated MT, does not occur until all cysteine residues are bound terminally, that is, considering Zn²⁺, after 5 Zn²⁺ have bound, Figure 17. Following this, bridging occurs to lead to the well known two-domain structure. Consequently, Zn₅-MT, where all twenty cysteine residues of MT are terminally coordinating five Zn²⁺ ions will not contain any free thiol groups. We summarise these mechanistic ideas in a metallation chart (Figure 17) that begins with metal-free MT, which progressively metallates to Zn₅-MT, at which point there are no free thiols. The key, and important new information on the mechanism is that only following this metallation point, do the addition of the 6th and 7th Zn²⁺s lead to the formation of first a single cluster then the familiar two-domain structure with 7 Zn²⁺ bound. The value of the models presented in this diagram is that it shows progressive metallation of the protein, and highlights the early stages of metallation (apo- to Zn₅-MT), which are important in the protection of an organism against oxidative stress, as well as the latter stages of metallation (Zn₇- to Cd₈-MT), which are important in protecting an organism against toxic metal insult and in maintaining the metal ion homeostasis of an organism.

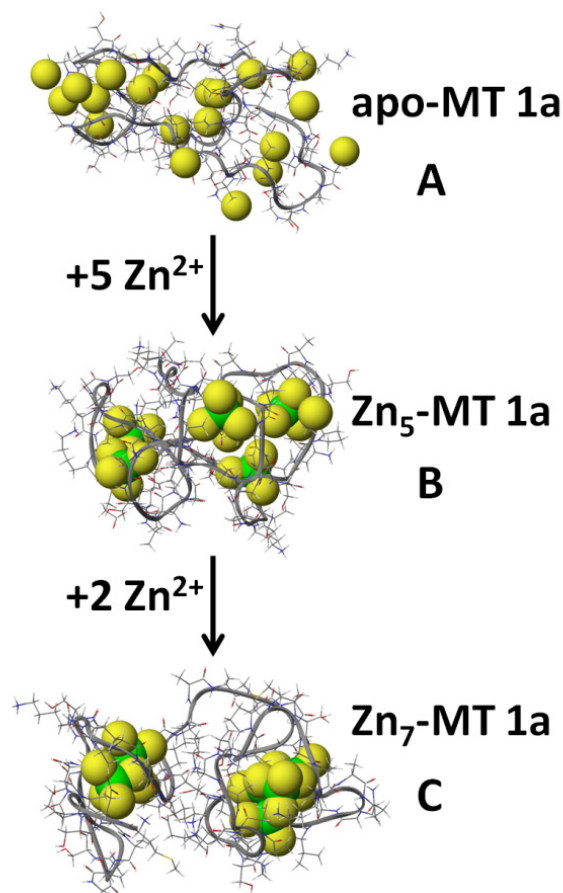


Figure 17. Molecular models of the metallation of MT from apo- to Zn₇-rhMT. Ribbons show the backbone, with zinc atoms represented as green spheres and sulphur atoms as yellow spheres. The N-terminal β -domain is located on the left hand side, while the C-terminal α -domain is located on the right-hand side. (A) Metal-free, apo- β -rhMT-1 showing an essentially spherical structure with the cysteinyl sulphurs on the outside. (B) The single domain Zn₅- β -rhMT structure. The structure was created by assigning a single Zn²⁺ ion to every 4 consecutive cysteine residues. (C) Formation of the filled two-domain cluster structure with addition of the 7th Zn²⁺ into the β -domain in Zn₇- β -rhMT. Structures were calculated using a locally modified force field with MM3/MD methods for molecular modelling¹⁰³. Minimization of each structure was carried out for 5000 ps at 300 K. The conformer with the lowest energy is presented above. The initial structure of the Cd₇- β -rhMT-1, modified for all subsequent structures, was provided by Chan et al.¹⁰⁴. Adapted with permission of ref³⁵ copyright (2013) American Chemical Society.

Metallothionein has been implicated in metal-ion homeostasis, in active redox control and as a protective agent against toxic metal insults³ and the schemes in Figures 17 and 18 provide a model for these roles.

With respect to the redox role, a metallothionein redox cycle, connecting oxidants with the redox silent Zn²⁺, has been suggested to account for the protective role of MT in the cell. Initially an ROS oxidizes MT leading to Zn²⁺ release. This Zn²⁺ then acts to upregulate Zn-dependent proteins, through MTF-1,

and subsequent reduction of MT using glutathione, or replacement with *de novo* synthesized MT and reestablishment of zinc homeostatic buffering¹¹¹. With the present results, one can now begin to assess the redox potential of the differently metallated versions of MT (Zn₁- to Zn₅-MT), and how metallation of all the cysteine residues, forming Zn₅-MT, affects its ability to act as a protective agent. It is possible that the subtle control of the redox activity of Zn₅-MT controls its biological activity - the change from terminal Cys to one free Cys (and therefore available SH groups) or additionally to a bridging Cys may be a low energy reaction allowing for active but controlled redox properties, Figures 17 and 18.

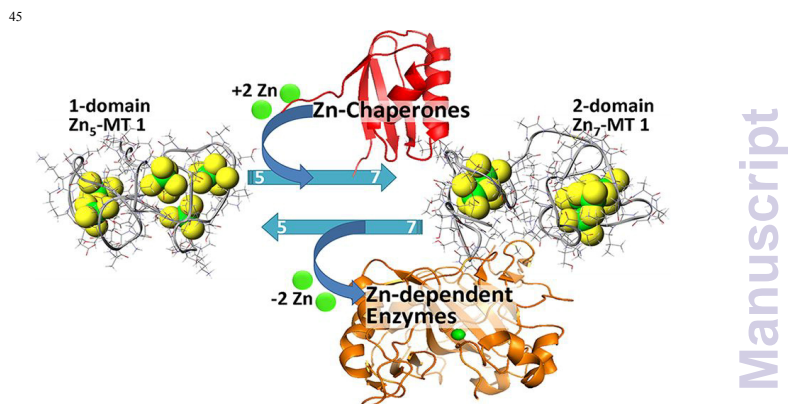


Figure 18. A summary of the role of Zn₅-MT in providing homeostatic control in cells. The Figure shows a model in which Zn₅-MT is the stable cellular species, two additional Zn²⁺ bind to form the well-known clusters within two-metal binding sites but with much lower binding affinities than the other 5 Zn²⁺ bound. The cluster-forming Zn's are readily available for metallation of Zn-dependent enzymes or transcription factors. Reprinted with permission of ref³⁵ copyright (2013) American Chemical Society.

This new model provides a mechanism for the homeostatic role because shuttling between the beaded and clustered structures allows for the ready transfer of Zn²⁺ to apo-metalloenzymes as shown in Figure 18.

hMT-1 is capable of binding an additional eighth Cd²⁺ ion to form Cd₈-MT-1^{30, 117}. This species is stabilized due to the higher affinity of Cd²⁺ ions for thiols, compared with Zn²⁺ ions. Unique to this structure is the bridging of both domains to coordinate the eighth metal ion. We propose that when the protein is fully metallated, such as Zn₇-MT-1, the incoming metal ion must be able to coordinate and expel a previously bound Zn²⁺. In the case of Zn₇-MT, the formation of a transient M₁Zn₇- β -rhMT-1 can be envisioned as an exogenous Cd²⁺, or Cu⁺, ion coordinating to Zn₇- β -rhMT-1, bridging both domains with subsequent rearrangement and expulsion of a previously bound Zn²⁺ ion.

A final aspect of this 'bead' model with its single domain of 5 terminally-coordinated metal ions is that rearrangement to the two-domain cluster structure readily can introduce domain specificity as the thermodynamic choice of which domain to form the first cluster is likely controlled by the metal. The equilibrium illustrated in Figure 18 provides a facile route to domain specific binding as the formation of the clustered domains with the arrival

of the 6th and 7th divalent metals requires a major rearrangement of the binding sites.

Acknowledgements

We gratefully acknowledge financial support from NSERC of Canada through a Canada Graduate Scholarship (to DEKS), and Discovery and Equipment Grants (to MJS). MJS also thanks many of his students who have worked on and have maintained their interest in the metallothionein projects for the last 20 years,

without your dedication, perseverance and loyalty, these latest results described here would not be possible. We specifically acknowledge Dr. Sharbari Lahiri for her vital assistance with different aspects of our work recently. We wish also to acknowledge Mr. Doug Hairsine who has continued to provide excellent technical assistance with the mass spectrometer over many years.

Notes and references

Department of Chemistry, The University of Western Ontario, London, ON, Canada. E-mail: martin.stillman@uwo.ca; web: www.stillmangroup.ca; tel: +1 519-661-382.

† Electronic Supplementary Information (ESI) available: [details of any supplementary information available should be included here]. See DOI: 10.1039/b000000x/

‡ Footnotes should appear here. These might include comments relevant to but not central to the matter under discussion, limited experimental and spectral data, and crystallographic data.

- 1 M. J. Stillman, *Coord. Chem. Rev.*, 1995, **144**, 461-511.
- 2 J. Chan, Z. Huang, M. E. Merrifield, M. T. Salgado and M. J. Stillman, *Coord. Chem. Rev.*, 2002, 319-339.
- 3 D. E. K. Sutherland and M. J. Stillman, *Metalloomics*, 2011, **3**, 444-463.
- 4 P. Babula, M. Masarik, V. Adam, T. Eckschlager, M. Stiborova, L. Trnkova, H. Skutkova, I. Provaznik, J. Hubalek and R. Kizek, *Metalloomics*, 2012, **4**, 739-750.
- 5 E. Freisinger, *Dalton Trans.*, 2008, 6663-6675.
- 6 C. A. Blindauer, *J. Inorg. Biochem.*, 2013, **121**, 145-155.
- 7 A. Galdes, M. Vasak, H. A. O'Hill and J. H. R. Kagi, *FEBS Lett.*, 1978, **92**, 17-21.
- 8 H. Rupp, W. Voelter and U. Weser, *FEBS Lett.*, 1974, **40**, 176-179.
- 9 M. Vasak, A. Galdes, H. A. O'Hill, J. H. R. Kagi, I. Bremner and B. W. Young, *Biochemistry*, 1980, **19**, 416-425.
- 10 M. Margoshes and B. L. Vallee, *J. Am. Chem. Soc.*, 1957, **79**, 4813-4814.
- 11 J. H. R. Kagi, in *Metallothionein III: Biological roles and medical implications*, eds. K. T. Suzuki, N. Imura and M. Kimura, Birkhauser Verlag, Basel, 1993, pp. 29-55.
- 12 N. J. Robinson, *Nat. Chem. Biol.*, 2008, **4**, 582-583.
- 13 A. Schmidt, M. Hagen, E. Schutze, A. Schmidt and E. Kothe, *J. Basic Microb.*, 2010, **50**, 562-569.
- 14 B. Gold, H. Deng, R. Bryk, D. Vargas, D. Eliezer, J. Roberts, X. Jiang and C. Nathan, *Nat. Chem. Biol.*, 2008, **4**, 609-616.
- 15 C. A. Blindauer and O. I. Leszczyszyn, *Nat. Prod. Rep.*, 2010, **27**, 720-741.
- 16 M. Capdevila, R. Bofill, O. Palacios and S. Atrian, *Coord. Chem. Rev.*, 2012, **256**, 46-62.
- 17 A. Sigel, H. Sigel and R. K. O. Sigel, *Metal ions in Life Sciences*, The Royal Society of Chemistry, Cambridge, 2011.
- 18 C. T. Hunt, Y. Boulanger, S. W. Fesik and I. M. Armitage, *Environ. Health Perspect.*, 1984, **54**, 135-145.
- 19 Y. Boulanger and I. M. Armitage, *J. Inorg. Biochem.*, 1982, **17**, 147-153.
- 20 Y. Boulanger, I. M. Armitage, K.-A. Miklossy and D. R. Winge, *J. Biol. Chem.*, 1982, **257**, 13717-13719.
- 21 W. Braun, M. Vasak, A. H. Robbins, C. D. Stout, G. Wagner, J. H. R. Kagi and K. Wuthrich, *Proc. Natl. Acad. Sci. USA*, 1992, **89**, 10124-10128.
- 22 R. W. Briggs and I. M. Armitage, *J. Biol. Chem.*, 1982, **257**, 1259-1262.
- 23 M. J. Stillman and A. J. Zelazowski, *J. Biol. Chem.*, 1988, **263**, 6128-6133.
- 24 A. J. Zelazowski, J. A. Szymanska, A. Y. C. Law and M. J. Stillman, *J. Biol. Chem.*, 1984, **259**, 12960-12963.
- 25 M. J. Stillman, W. Cai and A. J. Zelazowski, *J. Biol. Chem.*, 1987, **262**, 4538-4548.
- 26 M. J. Stillman, Z. Gasyna and A. J. Zelazowski, *FEBS Lett.*, 1989, **257**, 283-286.
- 27 M. J. Stillman, A. J. Zelazowski, J. Szymanska and Z. Gasyna, *Inorg. Chim. Acta* 1989, **161**, 275-279.
- 28 A. J. Zelazowski, Z. Gasyna and M. J. Stillman, *J. Biol. Chem.*, 1989, **264**, 17091-17099.
- 29 V. Calderone, B. Dolderer, H.-J. Hartmann, H. Echner, C. Luchinat, C. DelBianco, S. Mangani and U. Weser, *Proc. Natl. Acad. Sci. USA*, 2005, **102**, 51-56.
- 30 D. E. K. Sutherland, M. J. Willans and M. J. Stillman, *J. Am. Chem. Soc.*, 2012, **134**, 3290-3299.
- 31 T. T. Ngu, M. D. M. Dryden and M. J. Stillman, *Biochem. Biophys. Res. Commun.*, 2010, **401**, 69-74.
- 32 T. T. Ngu, A. Easton and M. J. Stillman, *J. Am. Chem. Soc.*, 2008, **130**, 17016-17028.
- 33 T. T. Ngu, J. A. Lee, T. B. J. Pinter and M. J. Stillman, *J. Inorg. Biochem.*, 2010, **104**, 232-244.
- 34 T. T. Ngu and M. J. Stillman, *J. Am. Chem. Soc.*, 2006, **128**, 12473-12483.
- 35 K. L. Summers, D. E. K. Sutherland and M. J. Stillman, *Biochemistry*, 2013, **52**, 2461-2471.
- 36 D. E. K. Sutherland, K. L. Summers and M. J. Stillman, *Biochemistry*, 2012, **51**, 6690-6700.
- 37 D. E. K. Sutherland, K. L. Summers and M. J. Stillman, *Biochem. Biophys. Res. Commun.*, 2012, **426**, 601-607.
- 38 G. W. Irvine and M. J. Stillman, *Biochem. Biophys. Res. Commun.*, 2013, **441**, 208-213.

- 39 D. E. K. Sutherland and M. J. Stillman, *Biochem. Biophys. Res. Commun.*, 2008, **372**, 840-844.
- 40 P. Palumaa, E. Eriste, O. Njunkova, L. Pokras, H. Jorvall and R. Sillard, *Biochemistry*, 2002, **41**, 6158-6163.
- 41 P. M. Gehrig, C. You, R. Dallinger, C. Gruber, M. Brouwer, J. H. Kagi and P. E. Hunziker, *Protein Sci.*, 2000, **9**, 395-402.
- 42 Y. Hathout, D. Fabris and C. Fenselau, *Int. J. Mass spectrom.*, 2001, **204**, 1-6.
- 43 X. Yu, M. Wojciechowski and C. Fenselau, *Anal. Chem.*, 1993, **65**, 1355-1359.
- 44 D. E. K. Sutherland, M. J. Willans and M. J. Stillman, *Biochemistry*, 2010, **49**, 3593-3601.
- 45 E. Freisinger, *J. Biol. Inorg. Chem.*, 2011, **16**, 1035-1045.
- 46 J. Loebus, E. A. Peroza, N. Bluthgen, T. Fox, W. Meyer-Klaucke, O. Zerbe and E. Freisinger, *J. Biol. Inorg. Chem.*, 2011, **16**, 683-694.
- 47 E. A. Peroza, A. A. Kaabi, W. Meyer-Klaucke, G. Wellenreuther and E. Freisinger, *J. Inorg. Biochem.*, 2009, **103**, 342-353.
- 48 A. H. Robbins, D. E. McRee, M. Williamson, S. A. Collett, N. H. Xuong, W. F. Furey, B. C. Wang and C. D. Stout, *J. Mol. Biol.*, 1991, **221**, 1269-1293.
- 49 B. Dolderer, H. Echner, A. Beck, H.-J. Hartmann, U. Weser, C. Luchinat and C. DelBianco, *FEBS J.*, 2007, **274**, 2349-2362.
- 50 R. Bofill, M. Capdevila and S. Atrian, *Metallomics*, 2009, **1**, 229-234.
- 51 H. Li and J. D. Otvos, *Biochemistry*, 1996, **35**, 13937-13945.
- 52 Y. Uchida, K. Takio, K. Titani, Y. Ihara and M. Tomonaga, *Neuron*, 1991, **7**, 337-347.
- 53 C. J. Quaife, S. D. Findley, J. C. Erickson, G. J. Froelick, E. J. Kelly, B. P. Zambrowicz and R. D. Palmiter, *Biochemistry*, 1994, **33**, 7250-7259.
- 54 G. Meloni, K. Zovo, J. Kazantseva, P. Palumaa and M. Vasak, *J. Biol. Chem.*, 2006, **281**, 14588-14595.
- 55 K. K. Kramer, J. T. Zoelle and C. D. Klaassen, *Toxicol. Appl. Pharmacol.*, 1996, **141**, 1-7.
- 56 K. K. Kramer, J. Liu, S. Choudhuri and C. D. Klaassen, *Toxicol. Appl. Pharmacol.*, 1996, **136**, 94-100.
- 57 Y. Manso, P. A. Adlard, J. Carrasco, M. Vasak and J. Hidalgo, *J. Biol. Inorg. Chem.*, 2011, **16**, 1103-1113.
- 58 J. T. Pedersen, C. Hureau, L. Hemmingsen, N. H. H. Heegaard, J. Ostergaard, M. Vasak and P. Faller, *Biochemistry*, 2012, **51**, 1697-1706.
- 59 C. J. Quaife, E. J. Kelly, B. A. Masters, R. L. Brinster and R. D. Palmiter, *Toxicol. Appl. Pharmacol.*, 1998, **148**, 148-157.
- 60 K. B. Nielson, C. L. Atkin and D. R. Winge, *J. Biol. Chem.*, 1985, **260**, 5342-5350.
- 61 M. M. Morelock, T. A. Cormier and G. L. Tolman, *Inorg. Chem.*, 1988, **27**, 3137-3140.
- 62 T. T. Ngu, S. Krecisz and M. J. Stillman, *Biochem. Biophys. Res. Commun.*, 2010, **396**, 206-212.
- 63 K. E. Rigby and M. J. Stillman, *Biochem. Biophys. Res. Commun.*, 2004, **325**, 1271-1278.
- 64 K. E. Rigby, J. Chan, J. Mackie and M. J. Stillman, *Proteins Struct. Funct. Bioinf.*, 2006, **62**, 159-172.
- 65 K. E. Rigby-Duncan and M. J. Stillman, *J. Inorg. Biochem.*, 2006, **100**, 2101-2107.
- 66 K. L. Summers, A. K. Mahrok, M. D. M. Dryden and M. J. Stillman, *Biochem. Biophys. Res. Commun.*, 2012, **425**, 485-492.
- 67 Y. Li and W. Maret, *J. Anal. At. Spectrom.*, 2008, **23**, 1055-1062.
- 68 B. A. Messerle, A. Schaffer, M. Vasak, J. H. R. Kagi and K. Wuthrich, *J. Mol. Biol.*, 1990, **214**, 765-779.
- 69 B. A. Messerle, A. Schaffer, M. Vasak, J. H. R. Kagi and K. Wuthrich, *J. Mol. Biol.*, 1992, **225**, 433-443.
- 70 A. Krezel and W. Maret, *J. Am. Chem. Soc.*, 2007, **129**, 10911-10921.
- 71 B. L. Zhang, W. Y. Sun and W. X. Tang, *J. Inorg. Biochem.*, 1997, **65**, 295-298.
- 72 J. H. R. Kagi and B. L. Vallee, *J. Biol. Chem.*, 1961, **236**, 2435-2442.
- 73 K. E. Rigby-Duncan and M. J. Stillman, *FEBS J.*, 2007, **274**, 2253-2261.
- 74 T. T. Ngu, J. A. Lee, M. K. Rushton and M. J. Stillman, *Biochemistry*, 2009, **48**, 8806-8816.
- 75 S. R. Sturzenbaum, P. Kille and A. J. Morgan, *FEBS Lett.*, 1998, **431**, 437-442.
- 76 M. G. Burgos, C. Winters, S. R. Sturzenbaum, P. F. Randerson, P. Kille and A. J. Morgan, *Environ. Sci. Technol.*, 2005, **39**, 1757-1763.
- 77 M. Galay-Burgos, D. J. Spurgeon, J. M. Weeks, S. R. Sturzenbaum, A. J. Morgan and P. Kille, *Biomarkers*, 2003, **8**, 229-239.
- 78 S. R. Sturzenbaum, O. Georgiev, A. J. Morgan and P. Kille, *Environ. Sci. Technol.*, 2004, **38**, 6283-6289.
- 79 T. T. Ngu, S. R. Sturzenbaum and M. J. Stillman, *Biochem. Biophys. Res. Commun.*, 2006, **351**, 229-233.
- 80 R. Riek, B. Precheur, Y. Wang, E. A. Mackay, G. Wider, P. Guntert, A. Liu, J. H. R. Kagi and K. Wuthrich, *J. Mol. Biol.*, 1999, **291**, 417-428.
- 81 C. A. Morris, B. Nicolaus, V. Sampson, J. L. Harwood and P. Kille, *Biochem. J.*, 1999, **338**, 553-560.
- 82 M. E. Merrifield, J. Chaseley, P. Kille and M. J. Stillman, *Chem. Res. Toxicol.*, 2006, **19**, 365-375.
- 83 S. Singh, A. Mulchandani and W. Chen, *Appl. Environ. Microbiol.*, 2008, **74**, 2924-2927.
- 84 N. J. Robinson, A. Gupta, A. P. Fordham-Skelton, R. R. D. Croy, B. A. Whitton and J. W. Huckle, *Proc. R. Soc. Lond. B*, 1990, **242**, 241-247.
- 85 C. A. Blindauer, M. D. Harrison, J. A. Parkinson, A. K. Robinson, J. S. Cavet, N. J. Robinson and P. J. Sadler, *Proc. Natl. Acad. Sci. USA*, 2001, **98**, 9593-9598.
- 86 C. A. Blindauer, M. Tahir-Razi, D. J. Campopiano and P. J. Sadler, *J. Biol. Inorg. Chem.*, 2007, **12**, 393-405.
- 87 O. I. Leszczyszyn, C. D. Evans, S. E. Keiper, G. Z. L. Warren and C. A. Blindauer, *Inorg. Chim. Acta*, 2007, **360**, 3-13.
- 88 C. A. Blindauer, N. C. Polfer, S. E. Keiper, M. D. Harrison, N. J. Robinson, P. R. R. Langridge-Smith and P. J. Sadler, *J. Am. Chem. Soc.*, 2003, **125**, 3226-3227.
- 89 W. A. Eaton, E. R. Henry, J. Hofrichter and A. Mozzarelli, *Nature Struct. Biol.*, 1999, **6**, 351-358.
- 90 N. Felitsyn, M. Peschke and P. Kebarle, *Int. J. Mass spectrom.*, 2002, **219**, 39-62.
- 91 P. Kebarle and U. H. Verkerk, *Mass Spectrom. Rev.*, 2009, **28**, 898-917.
- 92 A. Krezel and W. Maret, *Biochem. J.*, 2007, **402**, 551-558.

- 93 W. Feng, J. Cai, W. M. Pierce, R. B. Franklin, W. Maret, F. W. Benz and Y. J. Kang, *Biochem. Biophys. Res. Commun.*, 2005, **332**, 853-858.
- 94 H. Willner, M. Vasak and J. H. R. Kagi, *Biochemistry*, 1987, **26**, 6287-6292.
- 95 M. Vasak and J. H. R. Kagi, *Proc. Natl. Acad. Sci. USA*, 1981, **78**, 6709-6713.
- 96 M. Vasak, J. H. R. Kagi, B. Holmquist and B. L. Vallee, *Biochemistry*, 1981, **20**, 6659-6664.
- 97 M. Good, R. Hollenstein, P. J. Sadler and M. Vasak, *Biochemistry*, 1988, **27**, 7163-7166.
- 98 J. Ejinik, J. Robinson, J. Zhu, H. Forsterling, C. F. Shaw-III and D. H. Petering, *J. Inorg. Biochem.*, 2002, **88**, 144-152.
- 99 I.-K. Rhee, K. S. Lee and P. C. Huang, *Protein Eng.*, 1990, **3**, 205-213.
- 100 M. T. Salgado and M. J. Stillman, *Biochem. Biophys. Res. Commun.*, 2004, **318**, 73-80.
- 101 M. T. Salgado, K. L. Bacher and M. J. Stillman, *J. Biol. Inorg. Chem.*, 2007, **12**, 294-312.
- 102 Y. Yang, W. Maret and B. L. Vallee, *Proc. Natl. Acad. Sci. USA*, 2001, **98**, 5556-5559.
- 103 J. Chan, M. E. Merrifield, A. V. Soldatov and M. J. Stillman, *Inorg. Chem.*, 2005, **44**, 4923-4933.
- 104 J. Chan, Z. Huang, I. Watt, P. Kille and M. J. Stillman, *Can. J. Chem.*, 2007, **85**, 898-912.
- 105 M. F. Sanner, The Scripps Research Institute, La Jolla, California, 1996
http://mgl.scripps.edu/people/sanner/html/msms_man.html.
- 106 G. W. Irvine, K. L. Summers and M. J. Stillman, *Biochem. Biophys. Res. Commun.*, 2013, **433**, 477-483.
- 107 M. K. Mohammad, Z. Zhou, M. Cave, A. Barve and C. J. McClain, *Nutr. Clin. Pract.*, 2012, **27**, 8-20.
- 108 J. Jansen, W. Karges and L. Rink, *J. Nutr. Biochem.*, 2009, **20**, 399-417.
- 109 A. H. Colagar, E. T. Marzony and M. J. Chaichi, *Nutr. Res.*, 2009, **29**, 82-88.
- 110 B. Zhang, O. Georgiev, M. Hagmann, C. Gunes, M. Cramer, P. Faller, M. Vasak and W. Scaffner, *Mol. Cell. Biol.*, 2003, **23**, 8471-8485.
- 111 Y. J. Kang, *Exp. Biol. Med.*, 2006, **231**, 1459-1467.
- 112 K. M. Taylor, S. Hiscox, R. I. Nicholson, C. Hogstrand and P. Kille, *Sci. Signal*, 2012, **5**, 1-9.
- 113 D. E. K. Sutherland, Ph. D. Thesis (2012) "Structural motifs in metallothioneins", The University of Western Ontario, London, Ontario, Canada.
- 114 H. Wang, Q. Zhang, B. Cai, H. Li, K.-H. Sze, Z.-X. Huang, H.-M. Wu and H. Sun, *FEBS Lett.*, 2006, **580**, 795-800.
- 115 B. Roschitzki and M. Vasak, *Biochemistry*, 2003, **42**, 9822-9828.
- 116 G. Meloni, V. Sonois, T. Delaine, L. Guilloreau, A. Gillet, J. Teissie, P. Faller and M. Vasak, *Nat. Chem. Biol.*, 2008, **4**, 366-372.
- 117 G. Meloni, T. Polanski, O. Braun and M. Vasak, *Biochemistry*, 2009, **48**, 5700-5707.
- 118 B. Roschitzki and M. Vasak, *J. Biol. Inorg. Chem.*, 2002, **7**, 611-616.
- 119 K. E. Rigby-Duncan, C. W. Kirby and M. J. Stillman, *FEBS J.*, 2008, **275**, 2227-2239.
- 120 A. Z. Mason, N. Perico, R. Moeller, K. Thrippleton, T. Potter and D. Lloyd, *Mar. Environ. Res.*, 2004, **58**, 371-375.
- 121 T.-Y. Li, A. J. Kraker, C. F. Shaw-III and D. H. Petering, *Proc. Natl. Acad. Sci. USA*, 1980, **77**, 6334-6338.
- 122 W. Maret, K. S. Larsen and B. L. Vallee, *Proc. Natl. Acad. Sci. USA*, 1997, **94**, 2233-2237.
- 123 W. Lu and M. J. Stillman, *J. Am. Chem. Soc.*, 1993, **115**, 3291-3299.
- 124 J. Zeng, R. Heuchel, W. Schaffner and J. H. R. Kagi, *FEBS Lett.*, 1991, **279**, 310-312.
- 125 K. Zangger, G. Oz, J. D. Otvos and I. M. Armitage, *Protein Sci.*, 1999, **8**, 2630-2638.
- 126 Y. Manso, M. Serra, G. Comes, M. Giralto, J. Carrasco, N. Cols, M. Vasak, P. Gonzalez-Duarte and J. Hidalgo, *J. Neurosci. Res.*, 2010, **88**, 1708-1718.
- 127 E. J. Kelly, C. J. Quafe, G. J. Froelick and R. D. Palmiter, *J. Nutr.*, 1996, **126**, 1782-1790.
- 128 L. Cai, X.-K. Li, Y. Song and M. G. Cherian, *Curr. Med. Chem.*, 2005, **12**, 2753-2763.
- 129 H. Kodama and C. Fujisawa, *Metallomics*, 2009, **1**, 42-52.
- 130 M. Suzuki-Kurasaki, M. Okabe and M. Kurasaki, *J. Histochem. Cytochem.*, 1997, **45**, 1493-1501.
- 131 N. O. Narthey, J. V. Frei and M. G. Cherian, *Lab. Invest.*, 1987, **57**, 397-401.
- 132 A. R. Green, A. Presta, Z. Gasyna and M. J. Stillman, *Inorg. Chem.*, 1994, **33**, 4159-4168.
- 133 A. R. Green and M. J. Stillman, *Inorg. Chem.*, 1996, **35**, 2799-2807.
- 134 M. Vasak and J. H. R. Kagi, *Met. Ions Biol. Syst.*, 1983, **15**, 213-273.
- 135 P. D. Ellis, *Science*, 1983, **221**, 1141-1146.
- 136 R. A. Haberkorn, L. Que, W. O. Gillum, R. H. Holm, C. S. Liu and R. C. Lord, *Inorg. Chem.*, 1976, **15**, 2408-2414.
- 137 P. J. Sadler, A. Bakka and P. J. Beynon, *FEBS Lett.*, 1978, **94**, 315-318.
- 138 M. Capdevila, N. Cols, N. Romero-Isart, R. Gonzalez-Duarte, S. Atrian and P. Gonzalez-Duarte, *Cell. mol. life sci.*, 1997, **53**, 681-688.
- 139 K. B. Nielson and D. R. Winge, *J. Biol. Chem.*, 1984, **259**, 4941-4946.
- 140 H. Wang, H. Li, B. Cai, Z.-X. Huang and H. Sun, *J. Biol. Inorg. Chem.*, 2008, **13**, 411-419.
- 141 N. Romero-Isart, L. T. Jensen, O. Zerbe, D. R. Winge and M. Vasak, *J. Biol. Chem.*, 2002, **277**, 37023-37028.
- 142 J. D. Otvos and I. M. Armitage, *Proc. Natl. Acad. Sci. USA*, 1980, **77**, 7094-7098.